Universiteit
Leiden
The Netherlands

Squaramide-based supramolecular polymers : from self-assembly to in vivo application

Saez Talens, V.

Citation
Saez Talens, V. (2018, December 10). *Squaramide-based supramolecular polymers : from self-assembly to in vivo application*. Retrieved from https://hdl.handle.net/1887/67527

Version:	Not Applicable (or Unknown)
License:	Licence agreement concerning inclusion of doctoral thesis in the Institutional Repository of the University of Leiden
Downloaded from:	https://hdl.handle.net/1887/67527

Note: To cite this publication please use the final published version (if applicable).

Cover Page

Universiteit Leiden

The handle http://hdl.handle.net/1887/67527 holds various files of this Leiden University dissertation.

Author: Saez, Talens V.
Title: Squaramide-based supramolecular polymers : from self-assembly to in vivo application
Issue Date: 2018-12-10

CHAPTER 5

Biodistribution of squaramide-based supramolecular polymer nanoparticles in zebrafish embryos

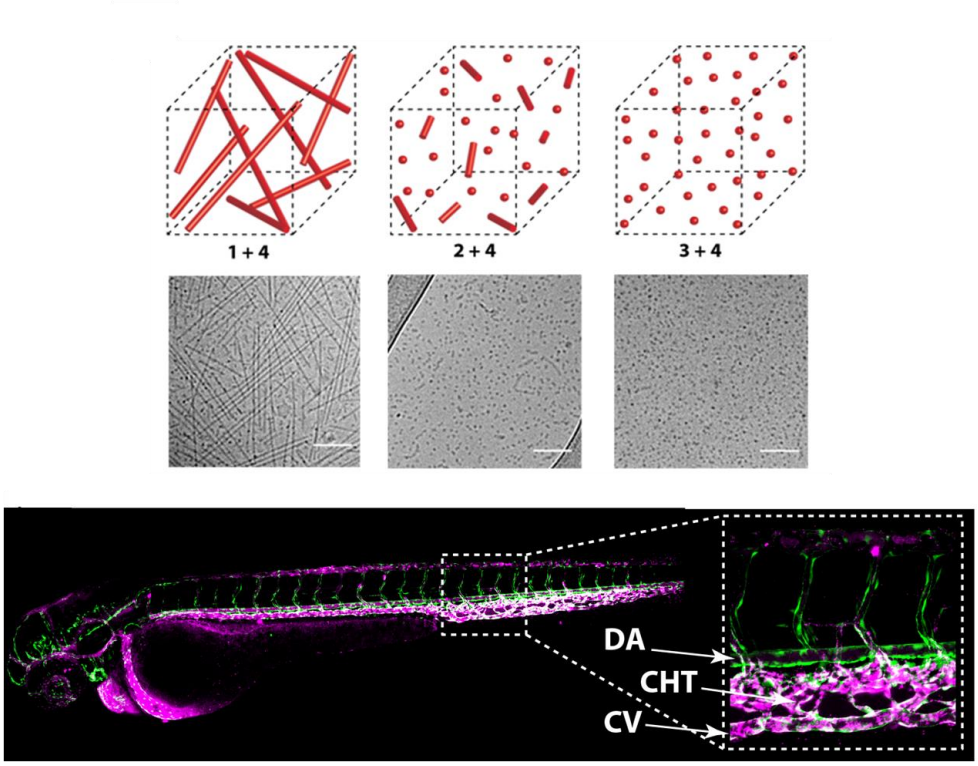

This chapter was prepared as an original research paper: Victorio Saez Talens, Gabriela Arias Alpizar, Jeroen Bussmann, Alexander Kros, Roxanne E. Kieltyka

5.1 Abstract

Supramolecular polymer biomaterials are attractive scaffolds to prepare nanoparticles for drug delivery due to their easy fabrication, and tunable shape and size. However, their exploitation as therapeutic nanocarriers until now has been limited, and a clear *in vivo* picture of their biodistribution and uptake remains challenging due to the opacity of the mammalian models used to study these processes. Here, I prepare fluorescently-labeled squaramide-based supramolecular polymer nanoparticles of varied shape, from fibrillar to spherical aggregates, and size, from hundreds to tens of nanometers, and tracking their *in vivo* biodistribution and uptake behavior once injected intravenously in a zebrafish embryo model. In all cases, the supramolecular polymer nanoparticles evaded macrophages, however they display distinct biodistribution consistent with particle type: spherical aggregates tens of nanometers in diameter circulate freely throughout the blood vessel lumen, whereas fibrillar aggregates several hundred nanometers in length were found to associate with scavenger endothelial cells that are functionally homologous to mammalian liver. Moreover, endothelial scavenging of the high aspect ratio self-assemblies was mediated largely through the Stabilin-2 transmembrane receptor as demonstrated previously for isotropic anionic nanoparticles. By applying a supramolecular approach based on squaramides for nanoparticle construction in combination with the transparent zebrafish embryo model, I show a facile means to generate cargo-loaded nanoparticles of various size and shape to establish such models as a first-line approach to probe biodistribution and mechanistic aspects of cellular uptake in the drug delivery community.

5.2 Introduction

Much effort has been dedicated to design and synthesize nanoparticulate (less than 500 nm in any dimension) carriers with precisely engineered physicochemical properties for the targeted delivery of therapeutics. To this end, particles of varied features including size, shape, surface charge, functionality, and elasticity have been prepared.[1–9] Irrespective of their designs it has been demonstrated that >99% of such particles are cleared by the liver, yet the cellular mechanisms by which these processes occur remain unclear due to the inherent difficulty to visualize them in mammalian models. A promising alternative to gain insight into the routing of such particles *in vivo* at the cellular level is the zebrafish (*Danio rerio*) embryo model system. This model system provides unparalleled opportunities in comparison to first-line mouse models used to assess the nanoparticle fate *in vivo* due their optical transparency, homology with 70% of human disease genes, easy manipulation with its fast development and external fertilization.[10–12] Recently, we have demonstrated the use of the zebrafish caudal vein to study processes related to nanoparticle uptake in the mammalian liver at the molecular level.[13] The sequestration and uptake of isotropic anionic nanoparticles was highly reliant on Stabilin-2, a transmembrane receptor on scavenger endothelial cells resident in the caudal vein, using *stab2* knockouts we validated the importance of this receptor for nanoparticle clearance in the liver.

Supramolecular self-assembly can provide access to a wide range of soft nanostructures, including those that are filamentous, through the polymerization of designed monomers using non-covalent interactions, such as hydrogen-bonding, aromatic interactions, electrostatic and/or hydrophobic effects.[5,14–21] This approach is of interest for applications in drug delivery because of its facile and modular character, where functional monomers can be combined in a mix-and-match fashion to prepare designed nanocarriers of varied physicochemical properties against a specific therapeutic target.[22–26] Although most studies involving supramolecular nanoparticles that are spherical or filamentous take place *in vitro*,[5,22,27,28] a number of in vivo studies have been executed in mouse models. [6,23,29–35] When their biodistribution is characterized, significant localization of the carrier is observed in the liver[36-40] as previously observed for inorganic nanoparticles.[7,42] However, it still remains unclear what physicochemical parameters are necessary to reduce their clearance by the liver. By combining a supramolecular approach to nanoparticle construction with the zebrafish embryo

model system, the door is opened to rapidly generate nanoparticle libraries to visually screen the nanoparticle-biological interface *in vivo* to unveil new opportunities to improve the systemic delivery of therapeutic payloads to their intended target.

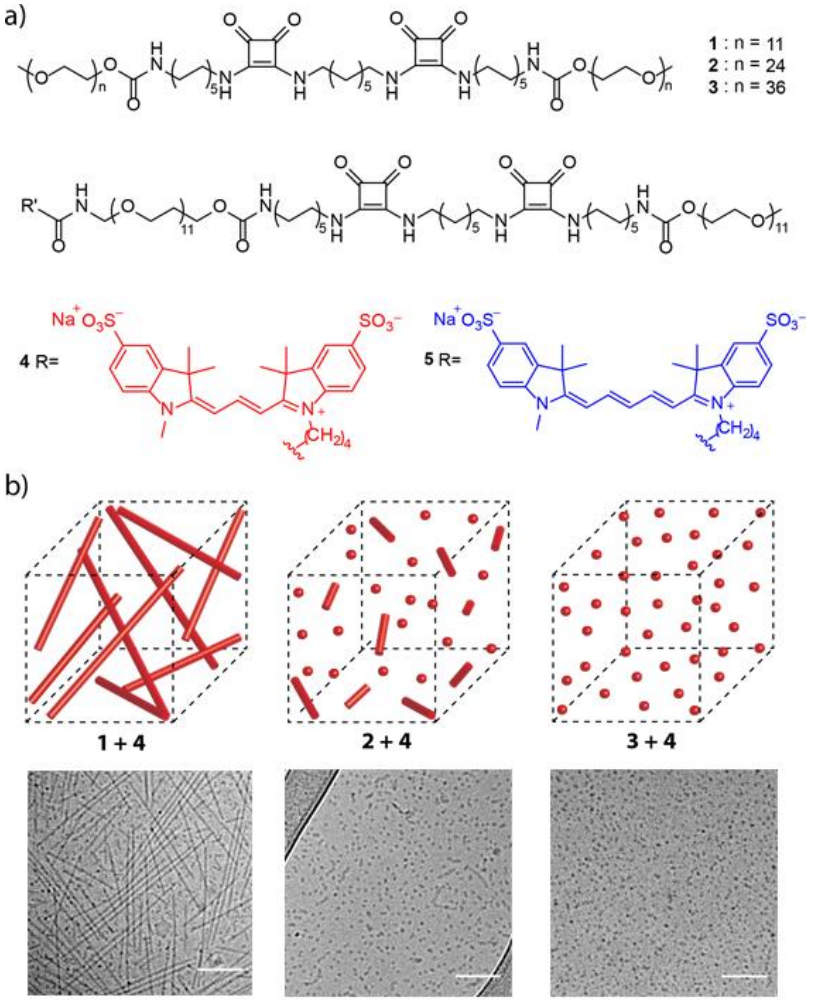

Figure 5.1. Squaramide-based bolaamphiphiles used to prepare supramolecular polymer nanoparticles for *in vivo* biodistribution studies. (a) Chemical structure of bolaamphiphile monomers **1**, **2** and **3** employed in the study to form fibrillar (**1**), mixed rod and spherical (**2**) or spherical (**3**) nanoparticles, respectively, upon self-assembly. The fluorescently-labeled squaramide-based monomer with a Sulfo-Cy3 dye (**4**) is used for tracking of the various supramolecular polymer nanostructures, while the Sulfo-Cy5 dye (**5**) is used in combination for fluorescence resonance energy transfer (FRET) experiments. (b) Schematic representation of the morphology of the co-assembled native (**1**, **2** or **3**) with dye-labeled monomer **4** (2 mol%) into fluorescently-labeled squaramide-based supramolecular polymer nanoparticles prior to injection into a zebrafish embryo model. Representative cryo-TEM images of co-assembled squaramide-based supramolecular polymer nanoparticles from native monomers (c = 2mM) **1**, **2** and **3** with **4** in water. Samples were prepared using the native squaramide-based bolaamphiphile monomer co-assembled with 2 mol% of Sulfo-Cy3 labeled squaramide-based bolaamphiphile **4**, displaying fiber-like structures for **1**, a mixture of spherical and rod-like structures for **2** and spherical aggregates for **3**. The scale bars represent 100 nm.

Earlier in our research group, we reported the self-assembly of a squaramide-based bolaamphiphile, consisting of monomer **1** (Figure 5.1a) into a supramolecular polymer nanoparticles in water.[42,43] Squaramides are ditopic hydrogen-bonding synthons that consist of a cyclobutenedione ring with two NH hydrogen bond donors opposite two carbonyl hydrogen bond acceptors[44] that benefit energetically from a gain in aromatic character upon self-assembly through hydrogen-bonding and hydrophobic interactions.[42,45,46] Classically, squaramides have been used in areas such as medicinal chemistry[47,48] catalysis[49,50] and bioconjugation,[51,52] however their application in polymers is underexplored. Recently, I have demonstrated the ability to tune the morphology of these squaramide-based supramolecular polymer nanoparticles from fibrillar to spherical by modulating the length of the oligo(ethylene glycol) (OEG) hydrophilic domain of the monomer: from n =11 resulting in fiber-like objects, to spherical aggregates with n = 36 (Figure 5.1a).[53] I herein report, the preparation of fluorescently-labeled squaramide-based supramolecular polymer nanoparticles with distinct shapes and sizes in aqueous media in order to tag and visually track their *in vivo* biodistribution and clearance by the Stabilin-2 receptor in a zebrafish embryo model to understand the range of this receptor in the clearance of nanoparticulate carriers for future drug delivery applications.

5.3 Results and discussion

Synthesis and co-assembly of fluorescently-labeled supramolecular polymer nanoparticles. The general molecular structure of the squaramide-based bolaamphiphile consists of two squaramides located within the center of its hydrophobic core surrounded by two hydrophilic oligo(ethylene glycol) oligomers at its opposite ends (**1**, **2** and **3**, Figure 5.1a). The two squaramide synthons are separated by an alkyl chain of seven methylene units, while an additional chain of ten methylene units are at the outer peripheries of the squaramide moieties. In this work, hydrophilic oligo(ethylene glycol) oligomers (OEG) of increasing chain length ((**1**) MW = 517 Da (n=11), (**2**) MW = 1089 Da (n=24) and (**3**) MW = 1617 Da (n=36)) were used to flank the hydrophobic core to drive the formation of supramolecular polymer nanoparticles of distinct shapes and sizes while providing a means to maintain the same surface chemistry. To be able to tag and track the various supramolecular polymer nanoparticles for their facile visualization in the transparent zebrafish embryo model system, an asymmetrically labeled squaramide-based bolaamphiphile, similar in molecular structure to **1**, with either

a fluorescent Sulfo-Cy3 (**4**) or a Sulfo-Cy5 (**5**) dye were synthesized. These molecules are predicted to co-assemble the fluorescently-labeled squaramide-based bolaamphiphiles because of their equally sized hydrophobic domains compared to the various supramolecular polymer nanoparticles containing distinct hydrophilic domains. Therefore, a single reporter monomer could be used for the labeling of the various structures under study.

Sulfonated variants of cyanine dyes were coupled to the monomers because of their increased solubility and introduced asymmetrically into the bolaamphiphile to reduce the potential for disruption of the formed supramolecular polymers or aggregation. The synthesis of the asymmetrically fluorescently-labeled squaramide-based bolaamphiphile was performed in a convergent manner, starting with the catalytic hydrogenation of O-(2-azidoethyl)undecaethylene glycol followed by Boc protection of the resulting amine group *in situ* using Boc-anhydride (see supporting information, section 5.6.4). Subsequently, the hydroxyl group of the heterobifunctional oligo(ethylene glycol) was activated using 1,1'-carbonyldiimidazole (CDI) and further reacted with N-Cbz-1,10-decanediamine and purified by reverse phase chromatography with a yield of 51%. Subsequently, catalytic hydrogenation of the Cbz protecting group led to the coupling of the amphiphile to 3,4-dibutoxy-3-cyclobutene-1,2-dione to provide a monosubstituted squaramide with a yield of 61% after purification by reverse-phase chromatography. The squaramide-based amphiphile with a Boc-protected amine at the OEG terminus was coupled to a second squaramide-based amphiphile with an internal C7-alkyl mono-Boc protected diamine chain and methoxy group at the OEG terminus on its periphery. The internal C7-alkyl mono-Boc protected diamine was deprotected under acidic conditions and then ligated to the squaramide-based amphiphiles with a Boc-protected amine under basic conditions with heating and purified by reverse-phase chromatography to yield the heterobifunctional squaramide-based bolaamphiphile in 36% yield. The sulfonated dyes were subsequently coupled to the squaramide-based bolaamphiphiles by Boc-deprotection of the terminal amine group and its reaction with the corresponding Sulfo-Cy3 or Sulfo-Cy5 NHS ester under basic conditions to yield **4** or **5** after HPLC, in a yield of 40-45%.

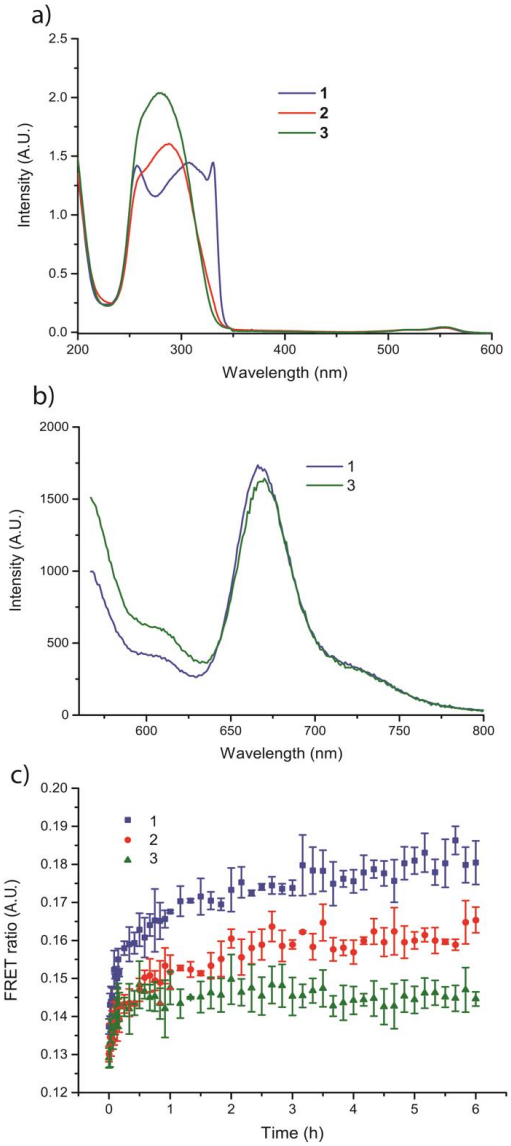

Figure 5.2. Spectroscopic studies of the self-assembled squaramide-based supramolecular polymer nanoparticles (c= 30 μM). (a) UV-Vis spectra of **1** (*blue line*), **2** (*red line*), and **3** (*green line*) co-assembled with **4 (**2 mol%). (b) Static measurements of **1** and **3** with an equimolar amount of **4** and **5** (2 mol% total of the dye-labeled monomers); FRET signal observed at 670 nm (c) Dynamic measurements of **1**, **2** and **3** co-assembled with **4** or **5** (2 mol% of each dye labeled monomer) independently and then mixed together in an equimolar ratio. FRET ratios are compared over time (6 h) for **1** (*blue line*), **2** (*red line*), and **3** (*green line*).

The fluorescently-labeled supramolecular polymer nanoparticles were prepared through co-dissolution of native squaramide-based bolaamphiphile (**1**, **2** or **3**) co-assembled with the Sulfo-Cy3 or Sulfo-Cy5 dye labeled squaramide-based bolaamphiphile (**4** or **5**, 2 mol%) in DMSO at experiment-specific concentrations. The samples were then lyophilized, reconstituted in water at room temperature and left to stand 24 hours prior to subsequent measurements. This facile mix-and-match preparation protocol involving monomer co-assembly can be used to prepare a library of supramolecular polymer nanoparticles with various physicochemical properties for applications in drug delivery.

Using a combination of microscopic and spectroscopic techniques, we first examined the potential of using a single, fluorescently-labeled monomer **4** for tagging of self-assemblies **1**-**3** with identical hydrophobic core lengths, but distinctly sized hydrophilic domains. In cryo-TEM measurements, highly disperse, fibrillar objects on the order of 282 ± 85 nm in length with a diameter of 6 ± 1 nm were observed for the co-assembly of **1** and **4** (Figure 5.1b, and Figure S5.7). The co-assembly of monomer **2** and **4** displayed a mixture of sphere and rod-like aggregate structures, similar to self-assembly of **2** on its own, with a diameter of 6 ± 1 nm, and comparable to the co-assembly of monomers **1** and **4** (Figure 5.1b and Figure S5.9). Conversely, supramolecular polymer nanoparticles of **3** and **4** displayed spherical objects in solution with a diameter of 9 ± 2 nm (Figure 5.1b and Figure S5.10). Surprisingly, monomer **4** also self-assembled on its own at the concentration used for co-assembly with **1**, **2**, or **3**, forming fibrillar aggregates with a length of 387 ± 194 nm. Remarkably, these fibrillar structures are not observed when monomer **4** is co-assembled with compounds **2** or **3,** suggesting that the dye-labeled monomers are likely inserted into the various self-assemblies. Moreover, the measured dimensions of the supramolecular polymer nanoparticles with the dye-labeled monomers are on par with cryo-TEM measurements of the self-assembled native monomers **1**, **2**, and **3**, indicating that they are unaffected by the incorporation of the dye-labeled monomer.[53]

UV-Vis spectroscopy measurements further supported the lack of disruption of the supramolecular polymer architecture at the molecular level upon co-assembly of **4** with the various native monomers (Figure 5.2a). Co-assembly of **1** and **4**, showed UV-Vis spectra comparable to native fibrillar self-assemblies of **1** with bands at 255 and 329 nm corresponding to the HOMO $\rightarrow$ (LUMO+1) and HOMO $\rightarrow$ LUMO transitions of the squaramide,[42] respectively (Figure 5.1a, and Figures

S5.2 and S5.3). Similar spectral traces were recorded for molecules **2** with **4** and **3** with **4** at the same molar ratio, with a lesser degree of blue- and red-shifting of the HOMO → (LUMO+1) and HOMO → LUMO bands when compared against **1** with **4**. This result highlights a likely difference in packing of the squaramide-based monomers within the self-assembled structures with increasing oligo(ethylene glycol) length. The spectral data for **2** and **3** with **4** are on par with those obtained for the native monomers that showed a decrease or absence of the band at 329 nm and a shoulder at 255 nm, yet self-assembly was observed.[53] Collectively, these results suggest that introduction of the fluorescent monomer into the prepared supramolecular polymer nanoparticles do not interfere with self-assembly of the native monomer.

Fluorescence resonance energy transfer (FRET) measurements were used to study incorporation of dye-labeled monomers into the supramolecular polymer nanoparticles (static measurements) and the rate of monomer exchange between nanoparticles (dynamic measurements). Static measurements were performed to measure the co-localization of monomers labeled with a Sulfo-Cy3 dye (molecule **4**, FRET donor) and those with a Sulfo-Cy5 dye (molecule **5**, FRET acceptor) at 1 mol% each with native monomers **1** or **3**. The co-assembly of monomers **1** or **3** with **4** and **5** resulted in an intermediate degree of FRET efficiency in comparison to other supramolecular polymers[27,54] by examining the acceptor emission at λ_{em} ≈ 670 nm (Figure 5.2b) against the fluorescence intensity of the donor emission λ_{em} ≈ 570 nm. However, a slightly higher degree of FRET efficiency was found for fibers of **1** in comparison to spherical aggregates of **3** and is consistent with their morphological differences. Overall, these results indicate that incorporation of both dye-labeled molecules into the supramolecular polymer nanoparticles occurs despite the distinct size of the hydrophobic domains presented by **1** or **3**.

Dynamic experiments were subsequently performed to understand the rate of monomer exchange between the supramolecular polymer nanoparticles. In these experiments, fluorescently-labeled supramolecular polymer nanoparticles were first prepared by the co-assembly of the native monomers **1**, **2** or **3** with 2 mol% of **4** or **5**. Subsequently, the distinctly labeled fluorescent nanoparticles with Sulfo-Cy3 or Sulfo-Cy5 were mixed and monomer co-localization within the fibers was measured by the evolution in FRET intensity over time. Monomer exchange between assemblies of **1**, **2** or **3** with **4** (Sulfo-Cy3) and assemblies (**1**, **2** or **3**) labeled with reporter molecule **5** (Sulfo-Cy5) were observed with different kinetic

profiles. Assemblies of **3** appeared to reach a plateau after 1 hour suggesting that the sample attained an equilibrium state in its exchange, whereas for **1** a plateau was still not reached after 6 hours. (Figure 5.2c) Qualitatively, the curves show a faster exchange of monomers in the case of the spherical aggregates (*green line*) composed of **3** compared to the fibrillar objects composed of **1** (*blue line*) (Figure 5.1c). However, in all cases the significantly lower FRET ratios observed in dynamic compared to the static measurements suggest that slow dynamics or a partial exchange of monomers[55] occurs within the fibers, but FRET experiments show the effective labeling of the supramolecular polymer nanoparticles by the Sulfo-Cy monomers.

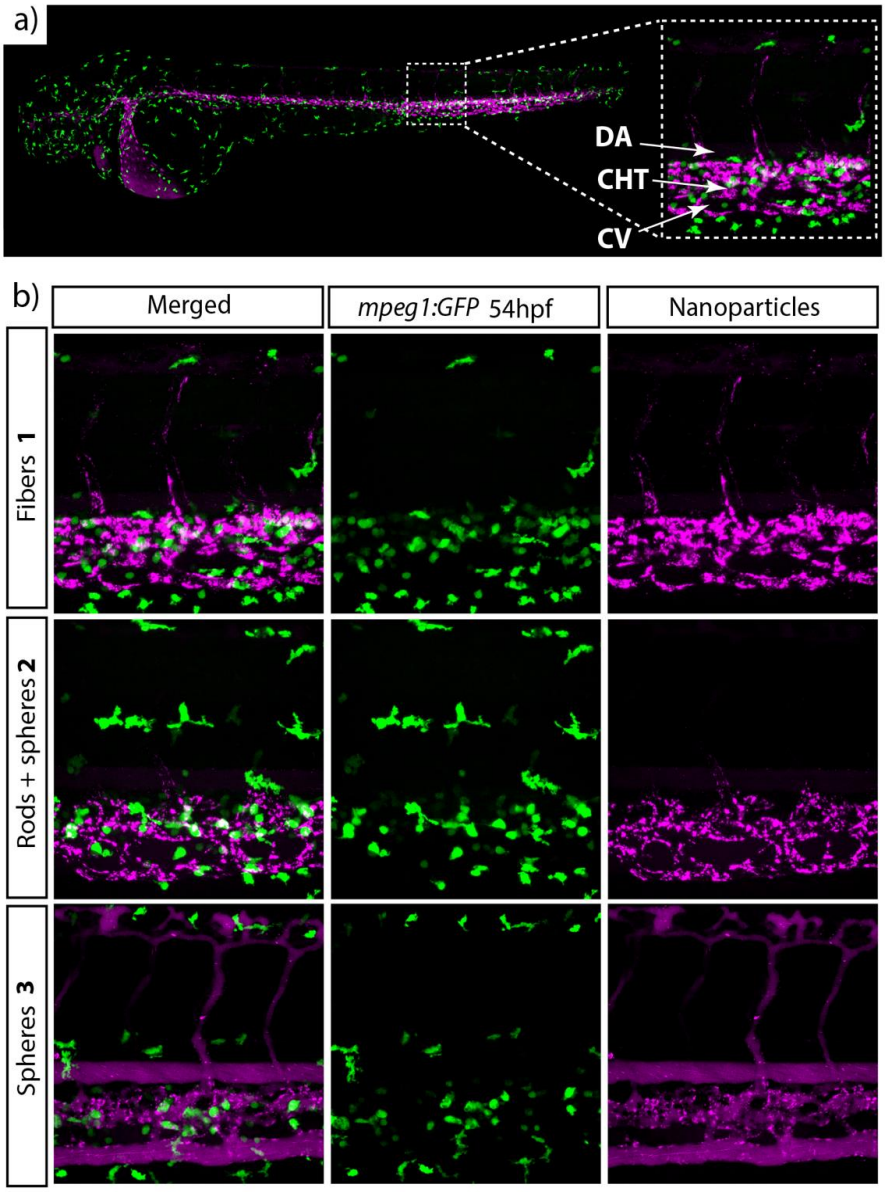

Figure 3. Colocalization studies of the fluorescently-labeled squaramide-based supramolecular polymer nanoparticles with macrophages in the zebrafish. a) Whole-embryo view after 1 hour injection in the Duct of Cuvier of **1** (c = 2 mM) co-assembled with **4** (2 mol%) in an embryonic zebrafish (mpeg1:GFP) at 54 hpf. In the boxed region, a zoom in of the caudal vein showing the dorsal aorta (DA), caudal hematopoietic tissue (CHT) and the caudal veins (CV). b) Fluorescently-labeled squaramide-based supramolecular polymer nanoparticles 1 hour post-injection in a transgenic zebrafish co-expressing GFP in macrophages. On the left panel, schematic representation of **1** (top), **2** (middle) and **3** (bottom) (c = 2 mM) with **4** (2 mol%). On the right panel, images of the CV area showing the in vivo distribution of each fluorescently-labeled squaramide-based supramolecular polymer nanoparticle tested.

Because the sulfonated-cyanine dyes used to fluorescently tag and track the supramolecular polymer nanoparticles bear a -1 formal charge, ζ-potential measurements were performed to estimate their surface charge in water. Negative ζ-potential values of -32.1 ± 7.1 mV were recorded for **4** that showed a fibrillar morphology (c = 40 μM) in cryo-TEM measurements on its own and used at this concentration for co-assembly experiments. Conversely, the co-assembly of native monomers **1**, **2**, or **3** with **4 (**2 mol%), resulted in near-neutral ζ-potential values of -4.9 ± 5.2 mV, -12.3 ± 4.7 mV and -11.1 ± 4.5 mV, respectively. As a control, the native monomer **1** (c = 2 mM) on its own showed similar ζ-potential values of -7.32 ± 5.5 mV and thus indicated that its co-assembly with monomer **4** was comparable in surface charge from the native self-assembled constructs. Hence, all investigated supramolecular polymer nanoparticles co-assembled with an anionic dye-labeled monomer were near-neutral in surface charge in comparison to **4** on its own that was negative.

Cumulatively, we demonstrate the co-assembly between a single sulfonated-cyanine (3 or 5) labeled fluorescent bolaamphiphile (**4**) and various native squaramide-based bolaamphiphiles of increasing OEG hydrophilic side chain lengths (**1**, n = 11; **2**, n = 24; and **3**, n= 36) to prepare fluorescently tagged supramolecular polymer nanoparticle self-assemblies. This mix-and-match strategy considerably reduces the synthetic effort to obtain libraries of functional assemblies by using a single cargo-loaded molecule that co-assembles with a variety of monomers.

***In vivo* evaluation of squaramide-based supramolecular polymer nanoparticles**. To establish the squaramide-based nanoparticles as potential drug carriers *in vivo*, zebrafish embryos were used between 52-56 hpf (hours post-injection). At this stage, blood circulation is robust and most organs, including liver and kidney have emerged. The stability of the supramolecular polymer nanoparticles was first assessed in biological media by monitoring their morphology in the presence of increasing concentration of carp serum (CS) concentration. Carp serum was used as the closest practical approximation to zebrafish serum. Diluted concentrations of CS, ranging from 1 to 25 v/v%, were probed to enable differentiation of the supramolecular polymer nanoparticles from the high background imposed by the serum components in cryo-TEM (Figure S5.7) measurements. Even in the presence of increasing CS concentrations, the supramolecular polymer nanoparticles consisting of **1** and **4** retained their respective morphologies and sizes relative to

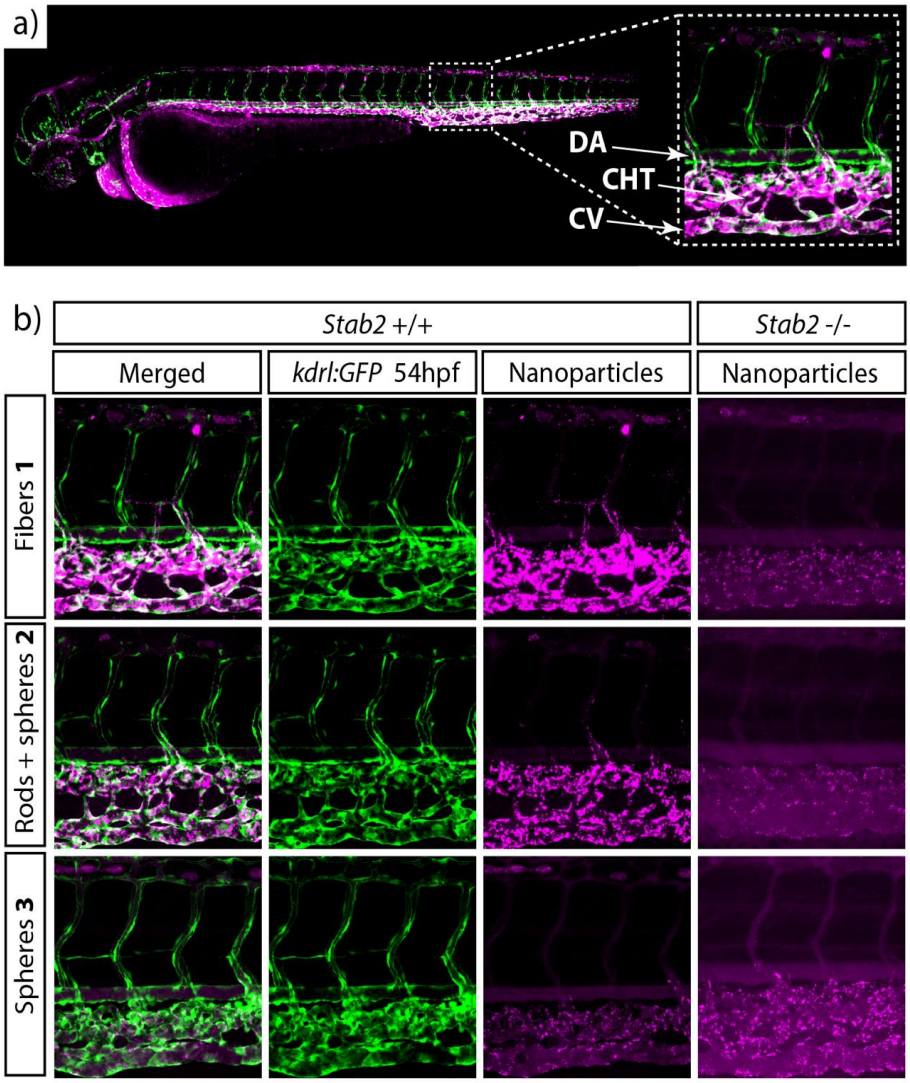

Figure 5.4. Biodistribution of the fluorescently-labeled squaramide-based supramolecular polymer nanoparticles in the zebrafish. a) Whole-embryo view 1 hour post-injection in the Duct of Cuvier of **1** (c = 2 mM) with **4** (2 mol%) in an embryonic zebrafish (kdrl:GFP) at 54 hpf. In the boxed region, the caudal vein showing the dorsal aorta (DA), caudal hematopoietic tissue (CHT) and the caudal veins (CV), zoomed in. b) Biodistribution of the three different fluorescently-labeled squaramide-based supramolecular polymer nanoparticles 1 hour post-injection. On the left panel, schematic representation of **1** (top) **2** (middle) and **3** (bottom) (c = 2 mM) with **4** (2 mol%). On the right panel, images of the CV area showing the distribution of each fluorescently-labeled squaramide-based supramolecular polymer nanoparticles. c) Biodistribution of **1** (top) **2** (middle) and **3** (bottom) (c = 2 mM) with **4** (2 mol%) in the zebrafish embryos lacking the stab2 receptor (stab2$^{-/-}$).

self-assemblies of the native monomer **1** (around several hundreds of nanometers in fiber length and a width between 5-6 nm by cryo-TEM), indicating that the serum components do not affect the formed co-assemblies (see Figure S5.11-S5.14). This result can be expected due to the high density of oligo(ethylene glycol)s on the periphery of the supramolecular polymer nanoparticles and the known use of such polymers to increase circulation time by reducing the interaction of nanoparticles with blood proteins.[56–58] However, samples of **2** or **3** with carp serum solutions of varied concentration could not be discriminated from the serum background due to their similar size and contrast.

Zebrafish embryos were first used to study macrophage uptake, since it is well established that this cell type plays an important role processing nanoparticles in an *in vivo* environment often hindering drug delivery through particle clearance.[13,41,59] Thus, transgenic zebrafish *Tg(mpeg:EGFP)^{gl22}* embryos in which GFP is expressed in macrophages were used, where colocalization indicates uptake of or binding to macrophages of the squaramide-based supramolecular polymer nanoparticles after intravenous injection. Remarkably, no significant co-localization of the supramolecular polymer nanoparticles and macrophages in the injected zebrafish was observed. This result can be explained by the dense presentation of oligo(ethylene glycol)s (MW ranging from 517 to 1617 Da) on the nanoparticle surface that may decrease protein absorption (Figure 5.3 and Figure S5.16). Hence, low protein absorption results in the evasion of macrophages by the squaramide-based supramolecular polymer nanoparticles.

Still, most of the supramolecular assemblies were rapidly removed from circulation (Figure 5.4). Most strikingly, the elongated fibrillar objects composed of the co-assembly of **1** and **4** showed limited free circulation with a preference for accumulation in a subset of venous endothelial cells (Figure 5.4a, 5.4b and Figure S5.15). Recently, we have shown that these cells in the zebrafish embryo are functionally homologous to the liver sinusoidal endothelial cells in mammals. In both zebrafish and mammals, these cells are specialized in endocytosis of macromolecular and nanoparticulate waste from circulation. Within these cells, the transmembrane scavenger receptor Stabilin-2 (*stab2*) plays a major role in mediating nanoparticle uptake from circulation.[13,60,61]

When we analyzed the nanoparticle distribution of the co-assembled supramolecular polymer nanoparticles composed of **1** and **4** in embryos lacking

the *stab2* receptor (*stab2*$^{-/-}$), their uptake by scavenger endothelial cells was largely abrogated. Similar results were observed for supramolecular polymer nanoparticles consisting of **2** and **4**, although this structure already displayed reduced uptake and increased circulation time relative to a co-assembly of **1** and **4** in control embryos. Interestingly, for the co-assembly of **3** and **4** only a slight accumulation in scavenger endothelial cells was observed in the knockout embryos, and uptake therefore appeared independent of *stab2* function (Figure 5.4b). Taken together, these results show that *stab2*-mediated nanoparticle uptake by scavenger endothelial cells is highly influenced by nanoparticle shape and/or size. Previously, shape-dependent circulation and distribution were reported for several nanoparticles,[6,35] but were mainly ascribed to differences in their hydrodynamic properties. By simultaneously exploiting the fluorescent labeling of the squaramide-based supramolecular polymer nanoparticles and the transparency of the zebrafish embryo model, we explore a mechanism for uptake of supramolecular polymer nanoparticles and show a major role for the sinusoidal scavenger receptor *stab2* that can be found analogously in the mammalian liver. This study shows for the first time the potential to track various supramolecular polymer architectures within the zebrafish embryo model to gain understanding of the molecular mechanisms governing the clearance of the nanoparticulate carriers of varied size and shape by liver sinusoidal endothelial cells.

5.4 Conclusions

In conclusion, a mix-and-match approach was used between native squaramide-based bolaamphiphiles of increasing hydrophilic chain lengths and a single asymmetrically-labeled fluorescent bolaamphiphile to prepare fluorescently tagged supramolecular polymer nanoparticles of distinct size and shape for their visual tracking *in vivo* in a zebrafish embryo model. These supramolecular polymer nanoparticles retained their shape and size after co-assembly with the fluorescent monomer in comparison to their native monomers, showed dynamic monomer exchange in FRET experiments, had near-neutral surface charge, and remained self-assembled in the presence of complex biological media such as carp serum. Additionally, the unique *in vivo* biodistribution of these variable aspect ratio squaramide-based supramolecular polymer nanoparticles were demonstrated in in zebrafish embryos. Fibrillar morphologies displayed a low circulation time with rapid venous attachment, whereas spherical morphologies demonstrated significantly greater mobility with longer circulation times and improved distribution over the zebrafish. These observations were rationalized by the

clearance of the particles by the scavenger endothelial cells through interaction with stabilin-2. Additionally, it was found that these supramolecular polymer nanoparticles also evaded macrophages. These results demonstrated that the nanocarrier shape and size, even at very high aspect ratios, plays an important role in nanoparticle clearance by scavenger endothelial cells through the Stabilin-2 receptor. The *in vivo* biodistribution behavior could be readily visualized in a zebrafish embryo model for the first time by simple fluorescent tagging using a co-assembly approach of functional monomers providing a synthetically efficient approach. It is anticipated that by understanding the *in vivo* routing of such fibrillar nanoparticles at the cellular level new chemical and/or biological strategies can be developed to improve payload delivery to a particular target.

5.5 References

(1) Nel, A. E.; Mädler, L.; Velegol, D.; Xia, T.; Hoek, E. M. V.; Somasundaran, P.; Klaessig, F.; Castranova, V.; Thompson, M. *Nat. Mater.* **2009**, *8* (7), 543–557.

(2) Bao, G.; Bazilevs, Y.; Chung, J.-H.; Decuzzi, P.; Espinosa, H. D.; Ferrari, M.; Gao, H.; Hossain, S. S.; Hughes, T. J. R.; Kamm, R. D.; Liu, W. K.; Marsden, A.; Schrefler, B. *J. R. Soc. Interface* **2014**, *11* (97), 20140301.

(3) Bozzuto, G.; Molinari, A. *Int. J. Nanomedicine* **2015**, *10*, 975–999.

(4) Simone, E. A.; Dziubla, T. D.; Muzykantov, V. R. *Expert Opin. Drug Deliv.* **2008**, *5* (12), 1283–1300.

(5) Webber, M. J.; Langer, R. *Chem. Soc. Rev.* **2017**, *46*, 6600–6620.

(6) Kinnear, C.; Moore, T. L.; Rodriguez-Lorenzo, L.; Rothen-Rutishauser, B.; Petri-Fink, A. *Chem. Rev.* **2017**, *117* (17), 11476–11521.

(7) Wilhelm, S.; Tavares, A. J.; Dai, Q.; Ohta, S.; Audet, J.; Dvorak, H. F.; Chan, W. C. W. *Nat. Rev. Mater.* **2016**, *1* (5), 16014.

(8) Wicki, A.; Witzigmann, D.; Balasubramanian, V.; Huwyler, J. *J. Control. Release* **2015**, *200*, 138–157.

(9) Petros, R. A.; DeSimone, J. M. *Nat. Rev. Drug Discov.* **2010**, *9* (8), 615–627.

(10) Lee, K. Y.; Jang, G. H.; Byun, C. H.; Jeun, M.; Searson, P. C.; Lee, K. H. *Biosci. Rep.* **2017**, *37* (3), BSR20170199.

(11) Chakraborty, C.; Sharma, A. R.; Sharma, G.; Lee, S.-S. *J. Nanobiotechnology* **2016**, *14* (1), 65.

(12) Santoriello, C.; Zon, L. I. *J. Clin. Invest.* **2012**, *122* (7), 2337–2343.

(13) Campbell, F.; Bos, F. L.; Sieber, S.; Arias-Alpizar, G.; Koch, B. E.; Huwyler, J.; Kros, A.; Bussmann, J. *ACS Nano* **2018**, *12* (3), 2138-2150.

(14) Krieg, E.; Bastings, M. M. C.; Besenius, P.; Rybtchinski, B. *Chem. Rev.* **2016**, *16*, 2414–2477.

(15) Boekhoven, J.; Stupp, S. I. *Adv. Mater.* **2014**, *26* (11), 1642–1659.

(16) Aida, T.; Meijer, E. W.; Stupp, S. I. *Science* **2012**, *335* (6070), 813–817.

(17) Webber, M. J.; Appel, E. A.; Meijer, E. W.; Langer, R. *Nat. Mater.* **2015**, *15* (1), 13–26.

(18) Appel, E. A.; del Barrio, J.; Loh, X. J.; Scherman, O. A. *Chem. Soc. Rev.* **2012**, *41* (18), 6195–6214.

(19) Leenders, C. M. A.; Baker, M. B.; Pijpers, I. A. B.; Lafleur, R. P. M.; Albertazzi, L.; Palmans, A. R. A.; Meijer, E. W. *Soft Matter* **2016**, *12* (11), 2887–2893.

(20) Busseron, E.; Ruff, Y.; Moulin, E.; Giuseppone, N. *Nanoscale* **2013**, *5* (16), 7098.

(21) Fernandez-Castano Romera, M.; Lafleur, R. P. M.; Guibert, C.; Voets, I. K.; Storm, C.; Sijbesma, R. P. *Angew. Chemie - Int. Ed.* **2017**, *56* (30), 8771–8775.

(22) Bakker, M. H.; Lee, C. C.; Meijer, E. W.; Dankers, P. Y. W.; Albertazzi, L. *ACS Nano* **2016**, *10* (2), 1845–1852.

(23) Soukasene, S.; Toft, D. J.; Moyer, T. J.; Lu, H.; Lee, H. K.; Standley, S. M.; Cryns, V. L.; Stupp, S. I. *ACS Nano* **2011**, *5* (11), 9113–9121.

(24) Straßburger, D.; Stergiou, N.; Urschbach, M.; Yurugi, H.; Spitzer, D.; Schollmeyer, D.; Schmitt, E.; Besenius, P. *ChemBioChem* **2018**, 10–15.

(25) Su, H.; Koo, J. M.; Cui, H. *J. Control. Release* **2015**, *219*, 383–395.

(26) Shamay, Y.; Shah, J.; Işlk, M.; Mizrachi, A.; Leibold, J.; Tschaharganeh, D. F.; Roxbury, D.; Budhathoki-Uprety, J.; Nawaly, K.; Sugarman, J. L.; Baut, E.; Neiman, M. R.; Dacek, M.; Ganesh, K. S.; Johnson, D. C.; Sridharan, R.; Chu,

K. L.; Rajasekhar, V. K.; Lowe, S. W.; Chodera, J. D.; Heller, D. A. *Nat. Mater.* **2018**, *17* (4), 361–368.

(27) Rho, J. Y.; Brendel, J. C.; Macfarlane, L. R.; Mansfield, E. D. H.; Peltier, R.; Rogers, S.; Hartlieb, M.; Perrier, S. *Adv. Funct. Mater.* **2017**, *1704569*, 1–11.

(28) Hinde, E.; Thammasiraphop, K.; Duong, H. T. T.; Yeow, J.; Karagoz, B.; Boyer, C.; Gooding, J. J. and Katharina Gaus, K. *Nat. Nanot.* **2017**, *12*, 81-91.

(29) Liu, J.; Liu, J.; Chu, L.; Zhang, Y.; Xu, H.; Kong, D.; Yang, Z.; Yang, C.; Ding, D. *ACS Appl. Mater. Interfaces* **2014**, *6* (8), 5558–5565.

(30) Webber, M. J.; Matson, J. B.; Tamboli, V. K.; Stupp, S. I. *Biomaterials* **2012**, *33* (28), 6823–6832.

(31) Toft, D. J.; Moyer, T. J.; Standley, S. M.; Ruff, Y.; Ugolkov, A.; Stupp, S. I.; Cryns, V. L. *ACS Nano* **2012**, *6* (9), 7956–7965.

(32) Dhandhukia, J. P.; Shi, P.; Peddi, S.; Li, Z.; Aluri, S.; Ju, Y.; Brill, D.; Wang, W.; Janib, S. M.; Lin, Y. A.; Liu, S.; Cui, H.; Mackay, J. A. *Bioconjug. Chem.* **2017**, *28* (11), 2715–2728.

(33) Moyer, T. J.; Kassam, H. A.; Bahnson, E. S. M.; Morgan, C. E.; Tantakitti, F., Chew, T. L., Kibbe, T. L. and Stupp, S. I. *Small* **2015**, *11* (23), 2750-2755.

(34) Bahnson, E. S. M.; Kassam, H. A.; Moyer, T.J.; Jiang, W.; Morgan, C. E.; Vercammen, J. M.; Jiang, Q.; Flynn, M. E.; Stupp, S. I. and Kibbe, M. R. *Antiox. and redox sign.* **2016**, 24 (*8*), 401-418.

(35) Geng, Y.; Dalhaimer, P.; Cai, S.; Tsai, R.; Tewari, M.; Minko, T.; Discher, D. E. *Nat. Nanotechnol.* **2007**, *2* (4), 249–255.

(36) Morgan, C.E.; Dombrowski, A.W.; Rubert Pérez, C.M.; Bahnson, E.S.; Tsihlis, N.D.; Jiang, W.; Jiang, Q.; Vercammen, J.M.; Prakash, V.S.; Pritts, T.A.; Stupp, S.I.; Kibbe, M.R. *ACS Nano.* **2016**, 10, (1), 899-909.

(37) Yang, C.; Chu, L.; Zhang, Y.; Shi, Y.; Liu, J.; Liu, Q.; Fan, S.; Yang, Z.; Ding, D.; Kong, D.; Liu, J. *ACS Appl. Mater. Interfaces* **2015**, *7* (4), 2735–2744.

(38) Zhang, S.; Zheng, Y.; Fu, D.; Li, W. Wu, Y. Li, B. and Wua, L. *J. Mater. Chem. B*, **2017**, 5, 4035-4043.

(39) Chen, D. and Sun J. *Polym. Chem.*, **2015**, 6, 998-1004

(40) Zhou, Z.; Xinpeng, M., Jin, E., Tang, J.; Sui, M.; Shen, Y.; Van Kirk, E. A.;

Murdoch, W. J. and Radosz, M. *Biomaterials* **2013**, *34*, 5722-5735.

(41) Tsoi, K. M.; Macparland, S. A.; Ma, X. Z.; Spetzler, V. N.; Echeverri, J.; Ouyang, B.; Fadel, S. M.; Sykes, E. A.; Goldaracena, N.; Kaths, J. M.; Conneely, J. B.; Alman, B. A.; Selzner, M.; Ostrowski, M. A.; Adeyi, O. A.; Zilman, A.; McGilvray, I. D.; Chan, W. C. W. *Nat. Mater.* **2016**, *15* (11), 1212–1221.

(42) Saez Talens, V.; Englebienne, P.; Trinh, T. T.; Noteborn, W. E. M.; Voets, I. K.; Kieltyka, R. E. *Angew. Chemie - Int. Ed.* **2015**, *54* (36), 10502–10506.

(43) Noteborn, W. E. M.; Saez Talens, V.; Kieltyka, R. E. *ChemBioChem* **2017**, 1995–1999.

(44) Ian Storer, R.; Aciro, C.; Jones, L. H. *Chem. Soc. Rev.* **2011**, *40* (5), 2330.

(45) Quiñonero, D.; Frontera, A.; Ballester, P.; Deyà, P. M. *Tetrahedron Lett.* **2000**, *41* (12), 2001–2005.

(46) Quiñonero, D.; Prohens, R.; Garau, C.; Frontera, A.; Ballester, P.; Costa, A.; Deyà, P. M. *Chem. Phys. Lett.* **2002**, *351* (1–2), 115–120.

(47) Ribeiro, C. J. A.; Espadinha, M.; Machado, M.; Gut, J.; Gonçalves, L. M.; Rosenthal, P. J.; Prudêncio, M.; Moreira, R.; Santos, M. M. M. *Bioorganic Med. Chem.* **2016**, *24* (8), 1786–1792.

(48) Olmo, F.; Rotger, C.; Ramírez-Macías, I.; Martínez, L.; Marín, C.; Carreras, L.; Urbanová, K.; Vega, M.; Chaves-Lemaur, G.; Sampedro, A.; Rosales, M. J.; Sánchez-Moreno, M.; Costa, A. *J. Med. Chem.* **2014**, *57* (3), 987–999.

(49) Malerich, J. P.; Hagihara, K.; Rawal, V. H. *J. Am. Chem. Soc.* **2008**, *130* (44), 14416–14417.

(50) Konishi, H.; Lam, T. Y.; Malerich, J. P.; Rawal, V. H. *Org. Lett.* **2010**, *12* (9), 2028–2031.

(51) Martínez, L.; Martorell, G.; Sampedro, Á.; Ballester, P.; Costa, A.; Rotger, C. *Org. Lett.* **2015**, *17* (12), 2980–2983.

(52) Owen, R. M.; Carlson, C. B.; Xu, J.; Mowery, P.; Fasella, E.; Kiessling, L. L. *ChemBioChem* **2007**, *8* (1), 68–82.

(53) Saez Talens, V.; Makurat, D. M. M.; Liu, T.; Noteborn, W. E. M.; Dai, W.; Guibert, C. L.; Voets, I. K.; Kieltyka, R. E. *Manuscr. Prep.*

(54) Baker, M. B.; Gosens, R. P. J.; Albertazzi, L.; Matsumoto, N. M.; Palmans, A. R. A.; Meijer, E. W. *ChemBioChem* **2016**, *17* (3), 207–213.

(55) da Silva, R. M. P.; van der Zwaag, D.; Albertazzi, L.; Lee, S. S.; Meijer, E. W.; Stupp, S. I. *Nat. Commun.* **2016**, *7*, 10.1038/ncomms11561.

(56) Knop, K.; Hoogenboom, R.; Fischer, D.; Schubert, U. S. *Angew. Chemie - Int. Ed.* **2010**, *49* (36), 6288–6308.

(57) Owens, D. E.; Peppas, N. A. *Int. J. Pharm.* **2006**, *307* (1), 93–102.

(58) Perry, J. L.; Reuter, K. G.; Kai, M. P.; Herlihy, K. P.; Jones, S. W.; Luft, J. C.; Napier, M.; Bear, J. E.; Desimone, J. M. *Nano Lett.* **2012**, *12* (10), 5304–5310.

(59) Bertrand, N.; Leroux, J. C. *J. Control. Release* **2012**, *161* (2), 152–163.

(60) Alidori, S.; Bowman, R. L.; Yarilin, D.; Romin, Y.; Barlas, A.; Mulvey, J. J.; Fujisawa, S.; Xu, K.; Ruggiero, A.; Riabov, V.; Thorek, D. L. J.; Ulmert, H. D. S.; Brea, E. J.; Behling, K.; Kzhyshkowska, J.; Manova-Todorova, K.; Scheinberg, D. A.; McDevitt, M. R. *Nat. Commun.* **2016**, *7*, 1–11.

(61) Miller, C. M.; Donner, A. J.; Blank, E. E.; Egger, A. W.; Kellar, B. M.; Østergaard, M. E.; Seth, P. P.; Harris, E. N. *Nucleic Acids Res.* **2016**, *44* (6), 2782–2794.

5.6 Supporting Information

5.6.1 Materials and methods

All reagents and chemicals were purchased from commercial sources and used without further purification. Sulfo-Cy3 and Sulfo-Cy5 dyes were obtained from Lumiprobe, while oligo(ethylene glycols) of various chain lengths (n= 11, 24, 36) were purchased from Broadpharm. Monomers **1**, **2** and **3** were synthesized as previously reported.[53] The synthetic protocol for the Sulfo-Cy3 and Sulfo-Cy5 squaramide-based bolaamphiphiles **4** and **5**, respectively, can be found in the Supporting Information. MilliQ water was used for all experiments. ζ-potential measurements were performed on a Zetasizer Nano ZS (Malvern). UV-Vis measurements were carried out on a Cary 300 UV-Vis spectrophotometer using a quartz cuvette with a path length of 1 cm. Fluorescence experiments were executed on an Infinite M1000 Pro Tecan plate reader using 96-well plate with a black background.

Preparation protocol of co-assembled sulfonated cyanine-labeled squaramide-based supramolecular polymer nanoparticles. Stock solutions of **1**, **2** or **3** were prepared at a concentration of 5.8 mM in DMSO, while stock solutions of **4** or **5** were prepared at a concentration of 0.2 mM in the same solvent. The native (**1**, **2** or **3**) and dye-labeled monomers (**4** or **5**) were mixed in a glass vial at the appropriate mol ratios (1 or 2 mol%). The solvent was lyophilized and the bolaamphiphile mixture was reconstituted in water at the desired concentration. The resulting clear solutions were left to stand for 24 hours prior to any measurement.

Cryogenic transmission electron microscopy (Cryo-TEM). Samples in water consisting of **1**, **2** or **3** (c = 2 mM) co-assembled with reporter molecule **4** (2 mol%), were prepared according to the co-assembly protocol above. The samples were left to stand for 24 hours before deposition on a glow discharged grid. Samples of **1** co-assembled with **4** (2 mol%) with increasing concentration of carp serum were prepared following a similar protocol. Instead of adding fresh water after removal of DMSO by lyophilization, a freshly prepared carp serum solution in water was added in the desired v/v% (ranging from 1 to 25 v/v%) to provide a final concentration of 2 mM of the fluorescently-labeled supramolecular polymer nanoparticle and left to stand 24 hours before deposition on a glow discharged grid. Cryo-TEM samples were prepared by depositing the sample (3 μL) on a glow

discharged Lacey Carbon Film (300 mesh Cu grids). The excess sample was removed by blotting for 1 second at room temperature with 95 % humidity (Whatman No.4 filter paper) and the resulting films were vitrified at -183 ºC using a Leica EMGP. Imaging of the samples was recorded with a Tecnai F20 FEG (FEI), equipped with a field emission gun at 200 kEV using a Gatan UltraScan camera with a defocus between -3 and -10 µm.

UV-Vis spectroscopy. UV-Vis samples in water consisting of **1**, **2** or **3** (c = 30 µM) co-assembled with **4** (2 mol%) were prepared according to the co-assembly protocol described above. The samples were left to stand for 24 hours before UV-Vis measurements.

Fluorescence spectroscopy (FRET measurements). The dye-labeled supramolecular polymers nanoparticles were prepared according to the co-assembly protocol mixing **1**, **2** or **3** (c = 30 µM) with **4** and/or **5** in different concentrations depending on the experiment. For static measurements: **4** and **5** (300 nM each) were mixed together in an equimolar ratio with native monomer (**1** or **3**) to obtain a total of 2 mol% of the fluorescently-labeled molecules in DMSO prior to lyophilization. After the reconstituted samples in water were left to stand overnight, they were loaded in a fluorimeter and excited at 550 nm (Sulfo-Cy3) and their fluorescence emission was measured from 570 to 800 nm (Sulfo-Cy5) at room temperature. Samples were measured in triplicate. For dynamic measurements: **4** or **5** (600 nM each) were mixed individually with the native monomer (**1**, **2** or **3**) to obtain mixtures of 2 mol% of the fluorescently-labeled molecule in DMSO prior to lyophilization. The equilibrated samples of the Sulfo-Cy3 and Sulfo-Cy5-labeled squaramide-based supramolecular polymer nanoparticles were mixed in a 1:1 ratio (100 µL each) in a 96-well plate by pipetting (2–3 x) with the acquisition of fluorescence data immediately after mixing at room temperature using excitation at 550 nm (Sulfo-Cy3) and measuring fluorescence emission from 570 to 800 nm (Sulfo-Cy5). The FRET ratio is the relative fluorescence intensity of the peaks at 670/570 nm. Experiments were run in triplicate to ensure reproducibility. Raw fluorescence data is provided in Figures S5.4 and S5.5 in the Supplementary Information.

ζ-potential measurements. Samples for electrophoretic mobility experiments were prepared from **1** or **1**, **2** or **3** (c = 2 mM) co-assembled with **4** (2 mol%) as outlined in the co-assembly protocol above. The samples were then transferred to

a reusable ζ-potential dip cell prior to measurement. The samples were left to stand for 24 hours before ζ-potential measurements.

Zebrafish husbandry and injections. Zebrafish (*Danio rerio*) were maintained and handled according to the guidelines from the Zebrafish Model Organism Database (http://zfin.org) and in compliance with the directives of the local animal welfare committee of Leiden University. Transgenic *Tg(kdrl:EGFP)*^{s843},[13] *Tg(mpeg:EGFP)*^{gl22} [13] and *stab2*^{ibl2} zebrafish[13] were used. Fertilization was performed by natural spawning at the beginning of the light period and eggs were collected and raised at 28.5 ºC in egg water (60 µg/mL Instant Ocean see salts). Pigment cell formation was suppressed by adding 1-phenyl-2-thiourea (PTU) to the egg water in 1-day old zebrafish (24-28 hpf).

Fluorescently-labeled squaramide-based supramolecular polymer nanoparticles were injected into 2-day old zebrafish embryos (52-56 hpf) using a modified microangraphy protocol described previously.[13] Embryos were anesthetized in 0.01% tricaine and embedded in 0.4% agarose containing tricaine before injection. Calibrated 1 nL volumes of squaramide-based supramolecular polymer nanoparticles consisting of native monomer **1**, **2** or **3** (c = 2 mM) co-assembled with **4** (2 mol%) were injected with a microneedle into the Duct of Cuvier. Successfully injected embryos were identified (damaged-yolk ball embryo excluded) and imaged using a Leica TCS SPE confocal microscope. Confocal micrographs (Z-stacks) for the whole embryo where generated using the 10x air objective (HCX PL FLUOTAR) and overlapping 3 images to cover the complete embryo, or a caudal vein by using 40x water-immersion objective (HCX APO L) to compare distribution of injected molecules. Images were processed using the Fiji, Image J Software and brightness/contrast adjusted.

5.6.2 Characterization methods

The reaction intermediates obtained in the synthesis of the squaramide-based bolaamphiphiles were purified using a Grace Reveleris X1 flash chromatography system equipped with a C18 column, while the final sulfonated cyanine-labeled squaramide-based bolaamphiphiles (**4** and **5**) were purified by RP-HPLC with a Vydac C18 reversed phase column. ^{1}H NMR and ^{13}C NMR spectra were acquired on a Bruker AV-III-600 MHz at 298K. LC-MS analysis was performed with a TSQ Quantum Access MAX system equipped with a Gemini 3 µm C18 110 Å 50×4.60 mm column (UV detection at 214 nm and 254 nm).

5.6.3 Synthetic route

The synthetic procedure for the sulfonated cyanine-labeled squaramide-based bolaamphiphiles is shown below. Squaramide-based bolaamphiphiles **1**, **2** and **3**, and intermediates **6** and **7** were reported elsewhere.[1]

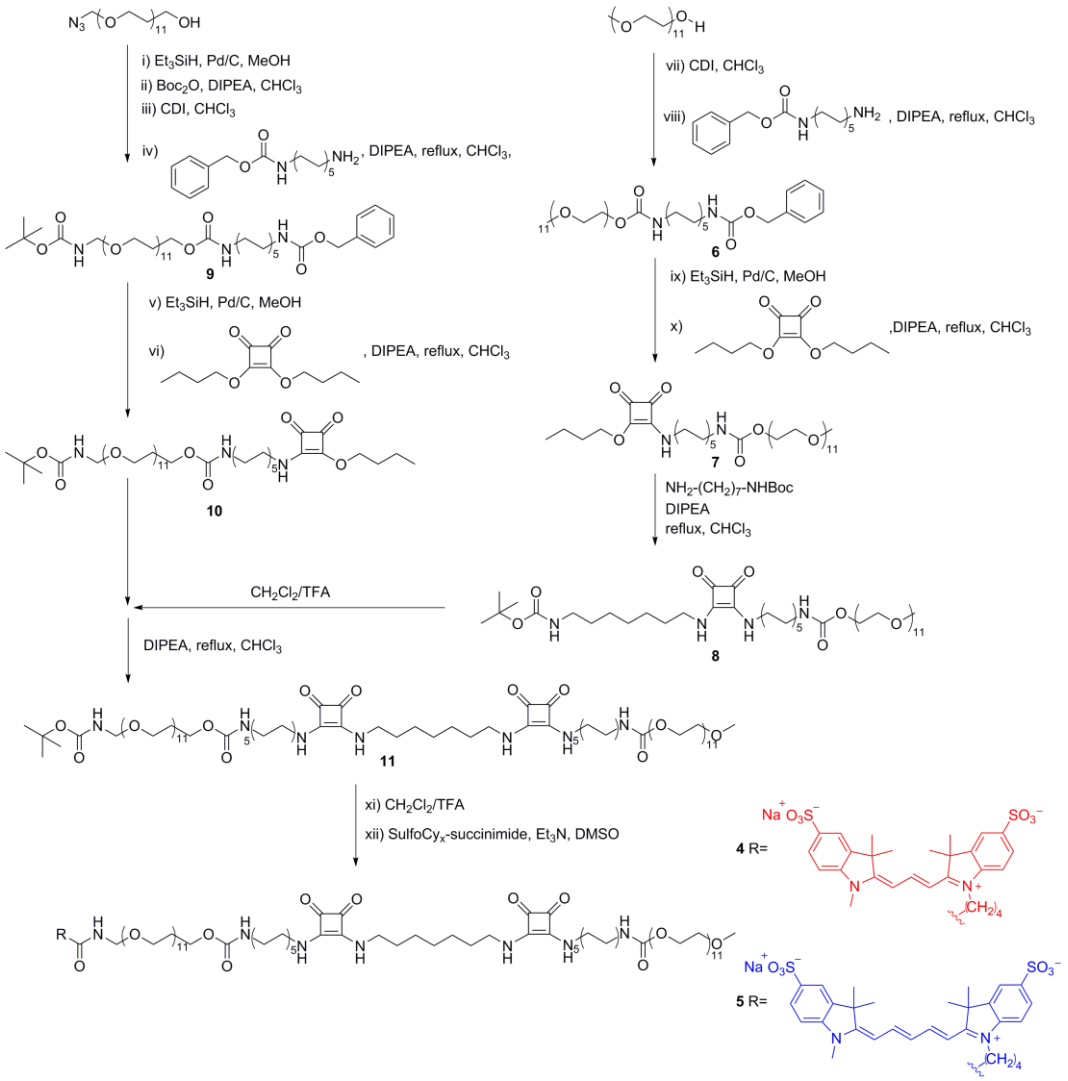

Scheme S5.1. Synthetic route for sulfonated cyanine-labeled monomers **4** and **5**.

Synthesis of 8

N-Boc-1,7-diaminoheptane (41.4 mg, 0.18 mmol) (synthesis reported elsewhere[2]) was added to a stirred mixture of **7** (106.0 mg, 0.12 mmol) and DIPEA (105.0 µL, 0.60mmol) in $CHCl_3$ (10 mL) refluxed overnight. The resulting compound was purified by reversed-phase C18 silica column using a gradient of 10-90% CH_3CN/H_2O over 45 minutes. The product was concentrated by evaporation and lyophilized to obtain a white solid.

Yield: 70.1 mg, 56.0% ^{1}H-NMR (δ_H[ppm], $CDCl_3$, 600 MHz): 7.46 (br s, 1H), 5.09 (br s, 1H), 4.83 (br s, 1H), 4.20-4.19 (m, 2H), 3.84-3.65 (m, 44H), 3.56-3.52 (m, 2H), 3.38 (s, 3H), 3.15-3.06 (m, 4H), 1.64-1.17 (m, 35H).^{13}C-NMR (δ_C[ppm], $CDCl_3$, 150 MHz): 183.43, 183.40, 169.02, 168.98, 157.58, 157.54, 80.10, 72.90, 72.82, 71.56, 71.53, 71.52, 71.49, 71.27, 70.99, 70.65, 64.81, 45.79, 45.60, 45.53, 42.04, 41.47, 32.19, 31.99, 30.94, 30.53, 30.46, 30.44, 30.31, 30.25, 30.23, 29.83, 29.47, 27.71, 27.58, 27.47, 27.37. LC-MS: t =6.67 min, *m/z*: 922.80 $[M+H\text{-}Boc]^+$.

Synthesis of 9

O-(2-Azidoethyl)undecaethylene glycol (0.6 g, 1.05 mmol) was dissolved in 5 mL MeOH and Pd/C (55.0 mg, 0.52 mmol)was added followed by briefly degassing the reaction mixture with argon. Triethylsilane (1.7 mL, 10.50 mmol) was added dropwise to the reaction mixture resulting in an effervescent solution, and was left stirring at room temperature for two hours. After deprotection, the intermediate was confirmed by LC-MS (t = 3.65 min, *m/z*: 546.13 $[M+H]^+$). Pd/C was removed by filtration over Celite, the reaction mixture was concentrated by rotary evaporation and dried with gentle stream of compressed air. Subsequently, O-(2-aminoethyl)undecaethylene glycol was Boc-protected using Boc-anhydride (0.3 g, 1.37mmol) and DIPEA (0.55 mL, 3.15mmol) in $CHCl_3$ (10 mL) upon stirring for 2 hours. The intermediate formation was verified by LC-MS (t = 4.73 min, *m/z*: 545.78 $[M+H\text{-}Boc]^+$). Next,1,1'-carbonyldiimidazole (0.29 g, 1.79 mmol) was added to the reaction mixture with stirring for an additional 2-3 hours to activate the hydroxyl group of the oligo(ethylene glycol) and verified by LC-MS(t = 7.57 min, *m/z*: 639.17 $[M+H\text{-}Boc]^+$). N-Cbz-1,10-decanediamine (0.42 g, 1.37 mmol) and DIPEA (0.37 mL, 2.10mmol) was added to the reaction mixture and refluxed overnight. The reaction mixture was purified by reversed-phase column chromatography using a 10-90% CH_3CN/H_2O gradient over 40 minutes. The final

product was concentrated by evaporation of CH_3CN followed by lyophilization of water to obtain compound **9** as a white solid.

Yield: 0.52 g, 50.6% ^{1}H-NMR (δ_H[ppm], $CDCl_3$, 600 MHz): 7.28-7.22 (m, 5H), 5.16 (br s, 1H), 5.07-5.05 (br s, 1H), 5.01 (s, 2H), 4.12 (t, 2H), 3.68-3.54 (m, 42H), 3.46-3.44 (t, 2H), 3.23-3.22 (m, 2H), 3.11-3.04 (m, 4H), 1.41-1.37 (m, 13H), 1.26-1.20 (m, 12H). ^{13}C-NMR (δ_C[ppm], $CDCl_3$, 150 MHz): 156.53, 156.09, 136.86, 128.50, 128.09, 128.04, 79.45, 72.72, 70.60, 70.55, 70.27, 69.70, 66.47, 63.78, 41.14, 41.06, 40.43, 29.97, 29.44, 29.25, 28.51, 26.75. LC-MS: t = 8.26min, *m/z*: 878.33[M+H-Boc]$^+$.

Synthesis of 10

Compound **9** (0.52 g, 0.53 mmol) was dissolved in MeOH (5 mL)and Pd/C (28.0 mg, 0.27 mmol) was added followed by briefly degassing the reaction mixture with argon.Triethylsilane (0.85 mL, 5.32 mmol) was added dropwise to the reaction mixture resulting in an effervescent solution, and was left stirring at room temperature for two hours. After Cbz-deprotection, the intermediate was confirmed by TLC-MS (*m/z*: 746.13 [M+H-Boc]$^+$), Pd/C was removed by filtration over Celite, concentrated by rotary evaporation and dried with gentle stream of compressed air.The crude product was redissolved in $CHCl_3$(10 mL) and 3,4-dibutoxy-3-cyclobutene-1,2-dione (149.0 µL, 0.69 mmol) and DIPEA (185.0 µL, 1.06 mmol) were added. The reaction mixture was refluxed overnight and subsequently, purified by C18 silica column using a gradient of 10-90% CH_3CN/H_2O over 40 minutes.The final product was concentrated by evaporation of CH_3CN followed by lyophilization of water to obtain a compound **10** as a white solid.

Yield: 0.42 g, 61.1% ^{1}H-NMR (δ_H[ppm], $CDCl_3$, 600 MHz): 5.18 (br s, 1H), 5.05 (br s, 1H), 4.75-4.73 (t, 2H), 4.21-4.20 (t, 2H), 3.76-3.61 (m, 42H), 3.56-3.53 (m, 2H), 3.42-3.37 (m, 2H), 3.31 (br s, 2H), 3.16-3.13 (m, 2H), 1.80-1.77 (m, 2H), 1.62-1.59 (m, 4H),1.48-1.44 (m, 15H), 1.31-1.28 (m, 12H),0.99-0.96 (t, 3H).^{13}C-NMR (δ_C[ppm], $CDCl_3$, 150 MHz): 190.45, 183.89, 178.41, 173.44, 157.47, 157.10, 80.17, 74.40, 72.88, 72.81, 72.64, 72.27, 71.48, 71.37, 71.35, 71.32, 71.25, 71.18, 71.08, 70.98, 70.83, 70.69, 67.91, 64.76, 64.66, 45.88, 45.42, 42.00, 41.34, 41.04, 40.90, 33.03, 32.06, 31.83, 31.63, 30.88, 30.33, 30.16, 30.05, 29.45, 27.66, 27.32, 19.67, 14.70. LC-MS: t = 7.38 min, *m/z*: 995.30 [M+H-Boc]$^+$.

Synthesis of 11

Trifluoroacetic acid (2 mL) was added to facilitate deprotection of the Boc-protecting group of **8** (31.8 mg, 0.031 mmol) for 20 minutes, and verified by LC-MS(t = 6.67min, *m/z*: 922.80 $[M+H\text{-}Boc]^+$).Afterwards, the solvent was evaporated by using a gentle stream of compressed air and the compound was redissolved in $CHCl_3$ (5 mL) with DIPEA (0.5 mL), and **10** (40.1 mg, 0.041 mmol) was added prior to refluxing the reaction mixture overnight. The compound was purified by C18 column chromatography using a gradient of 10-90% CH_3CN/H_2O over 25 minutes.The final product was concentrated by evaporation of CH_3CN followed by lyophilization of water to obtain a compound **11** as a white solid.

Yield: 20.4 mg, 35.6% ^{1}H-NMR (δ_H[ppm], $CDCl_3$, 600 MHz): 7.76 (br s, 1H), 7.52 (br s, 1H), 5.04 (br s, 1H), 4.21-4.20 (m, 4H), 3.69-3.54 (m, 94H), 3.39 (s, 3H), 3.32 (br s, 1H), 3.15 (m, 4H), 1.67-1.64 (m, 8H), 1.48-1.27 (m, 45H).^{13}C-NMR (δ_C[ppm], $CDCl_3$, 150 MHz): 183.62, 182.51, 170.00, 168.11, 157.54, 80.19, 72.92, 71.57, 71.54, 71.53, 71.49, 71.25, 70.68, 64.81, 60.04, 45.80, 44.21, 42.08, 41.39, 32.17, 30.98, 30.47, 30.27, 30.25, 29.46, 27.76, 27.43, 25.72. LC-MS: t = 6.73 min, 1745.55 *m/z*: $[M+H\text{-}Boc]^+$.

Synthesis of 4

Compound **11** (4.5 mg, 0.0024 mmol) was deprotected using a mixture of trifluoroacetic acid (1 mL) for 20 minutes. Deprotection of the Boc-group was confirmed by LC-MS (t= 5.77 min, m/z: 1745.27 $[M+H]^+$) and the solvents were evaporated by a gentle stream of compressed air before being redissolved in DMSO (1.5 mL). Triethylamine (250 µL) was added to the stirring solution along with Sulfo-Cy3 NHS ester (2.12 mg, 0.0036 mmol). MilliQ water (3.5 mL) was added to the reaction mixture and dialyzed against water using a dialysis bag with a molecular weight cut off (MWCO)= 1000 Da. The compound was purified by reversed-phase HPLC using a C18 column and a gradient of 10-90% CH_3CN/H_2O over 25 minutes. The product fractions were collected and lyophilized to yield compound **4** as a sticky pink material.

Yield: 2.36 mg, 45.01%. LC-MS: t = 5.83 min, *m/z*: 2345.1 $[M+H]^+$.

Synthesis of 5

Compound **11** (4.5 mg, 0.0024 mmol) was Boc-deprotected with a mixture of trifluoroacetic acid (1 mL) for 20 minutes. Deprotection of the Boc-group was confirmed by LC-MS (t= 5.77 min, m/z: 1745.27 $[M+H]^+$) and the solvents were evaporated by a gentle stream of compressed air before being redissolved in DMSO (1.5 mL). Triethylamine (250 µL) was added to the stirring solution along with Sulfo-Cy5 NHS ester (2.2 mg, 0.0036 mmol). MilliQ-water was added to the reaction mixture and dialyzed against water using a dialysis bag with a molecular weight cut off (MWCO)= 1000 Da. The compound was purified by reversed-phase HPLC using a C18 column and a gradient of 10-90% CH_3CN/H_2O over 25 minutes. The product fractions were collected and lyophilized to yield compound **4** as a sticky dark blue material.

Yield: 2.13 mg, 40.14%. LC-MS: t = 5.87 min, *m/z*: 2372.03 $[M+H]^+$.

5.6.4. Cryo-TEM of 4

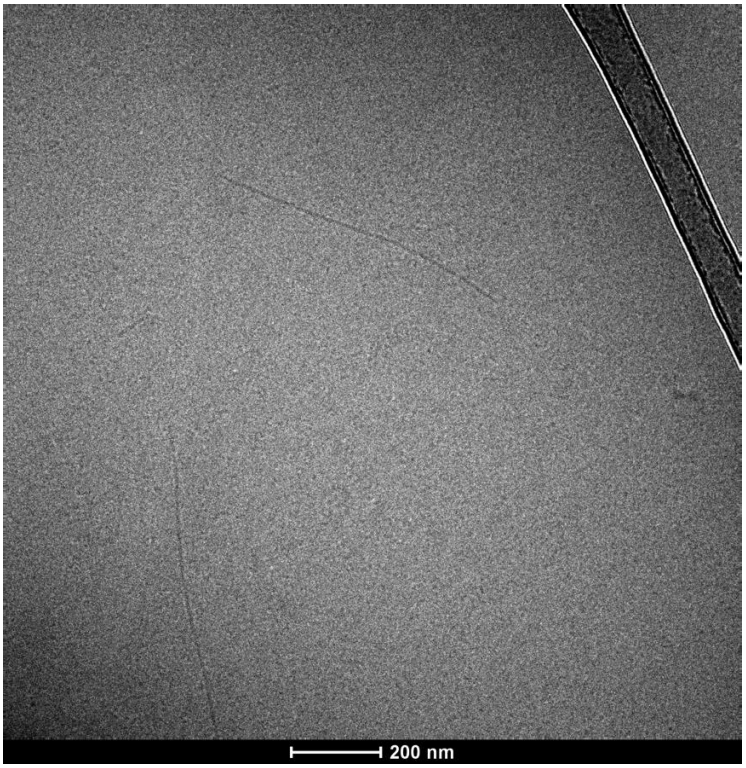

Figure S5.1. Cryogenic transmission electron microscopy (cryo-TEM) of **4** (c = 40 µM) on its own in water, as a control. Fibrillar aggregates are observed.

5.6.5 UV-Vis spectra

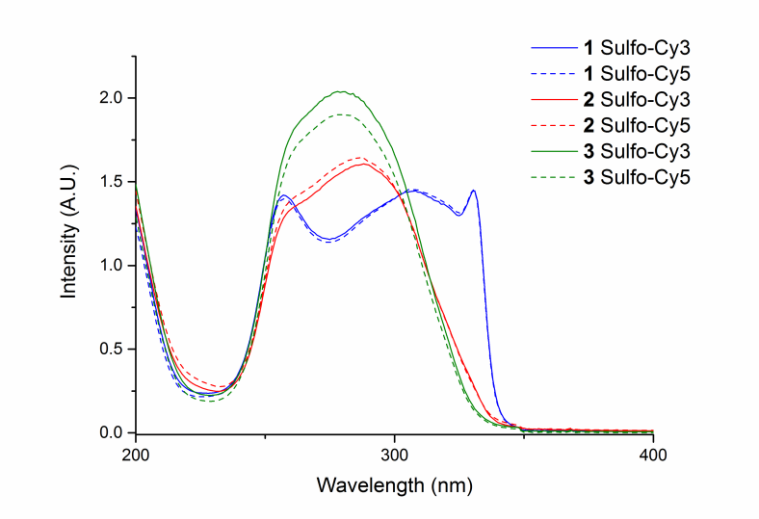

Figure S5.2. UV-Vis spectrum (200-400 nm) of **1**, **2** and **3** (c =30µM) with 2 mol% **4** (solid line) and **5** (dashed line).

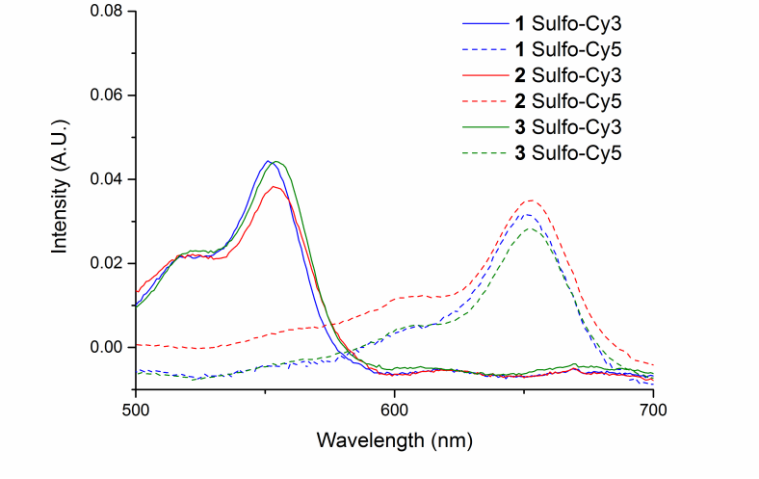

Figure S5.3. UV-Vis spectrum (500-700 nm)of **1**, **2** and **3** (c = 30 µM) with 2 mol% **4** (solid line) and **5** (dashed line).

5.6.6. Fluorescence spectra

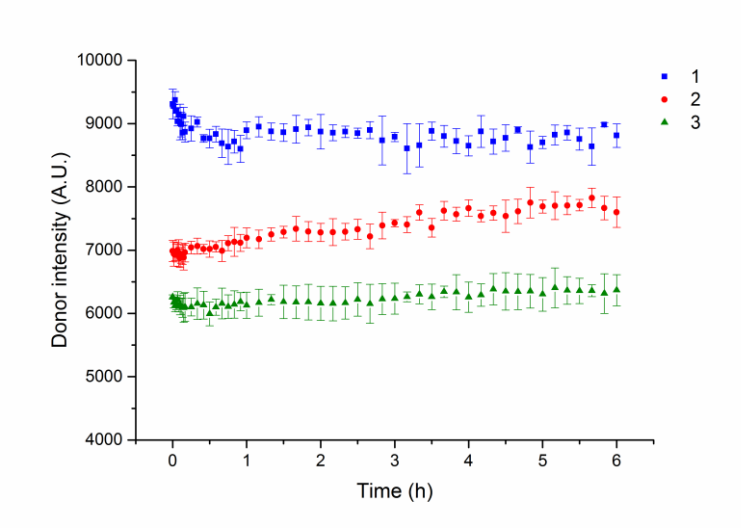

Figure S5.4. Raw fluorescent data from the donor (λ_{exc}= 550 nm λ_{em}= 570 nm) channel from FRET dynamic experiments where solutions containing **1** (blue), **2** (red) and **3** (green) labeled with **4** or **5** (2 mol%) are mixed in an equimolar ratio at room temperature.

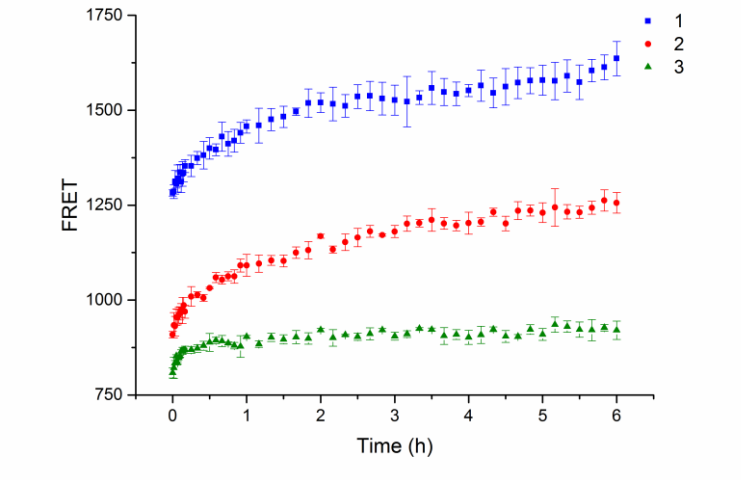

Figure S5.5. Raw fluorescence data (λ_{exc}= 550 nm λ_{em}= 670 nm) measuring the FRET channel in dynamic experiments where solutions of **1** (blue), **2** (red) and **3** (green) labeled with **4** or **5** (2 mol%) are mixed in an equimolar ratio at room temperature.

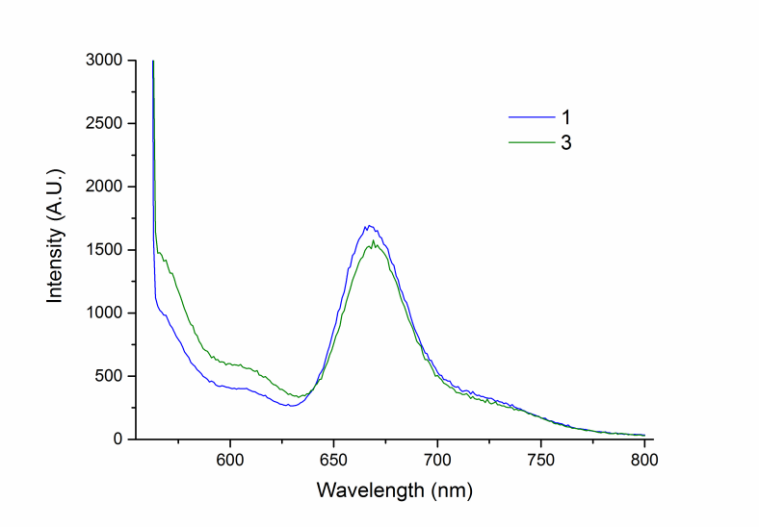

Figure S5.6. Static FRET measurements (zoom in, from 560 to 800 nm) of **1** and **3** with an equimolar amount of **4** and **5** (2 mol% total of the dye-labeled monomers); FRET signal observed at 670 nm.

3.5.7 Cryo-TEM of 1 with carp serum

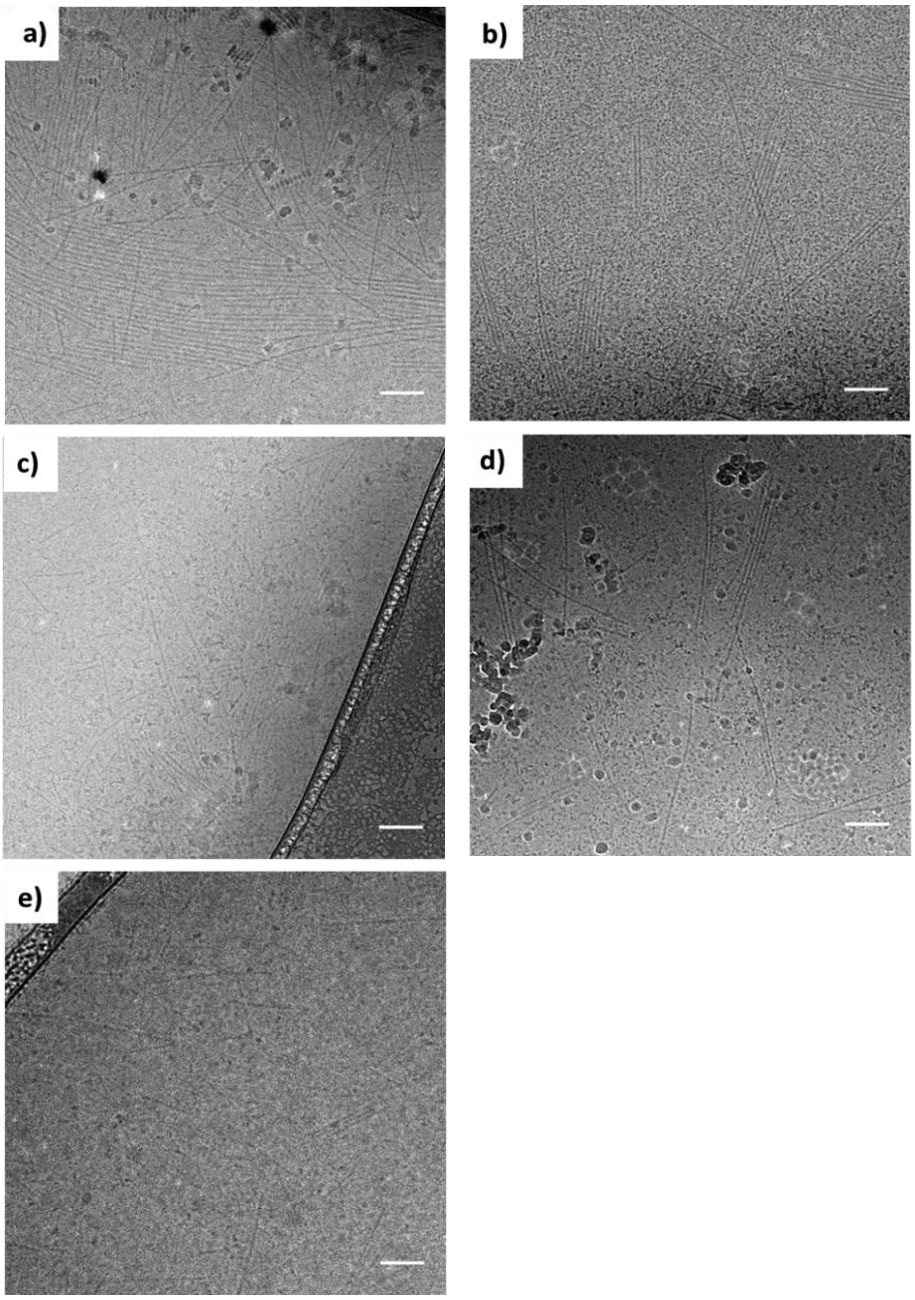

Figure S5.7. Cryo-TEM images of squaramide-based supramolecular polymer nanoparticles of **1** (c = 2 mM) with 2 mol% **4** in a solution with increasing carp serum from 1-25 v/v%: 1% (a), 2.5% (b), 5% (c), 10% (d) and 25% (e). Fibrillar structures are retained with increasing carp serum concentration. Scale bar: 100 nm.

3.5.8 Supramolecular polymer nanoparticles length and width distributions

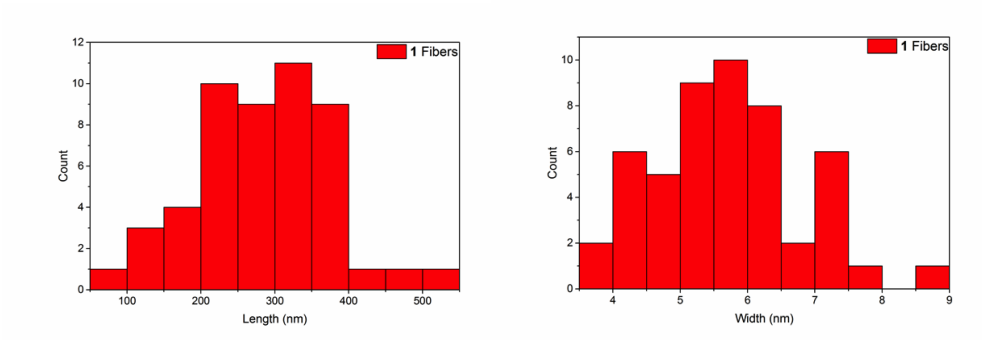

Figure S5.8. Histograms of length (282± 84 nm) and width (6 ± 1 nm) distributions measured for **1** (N = 50).

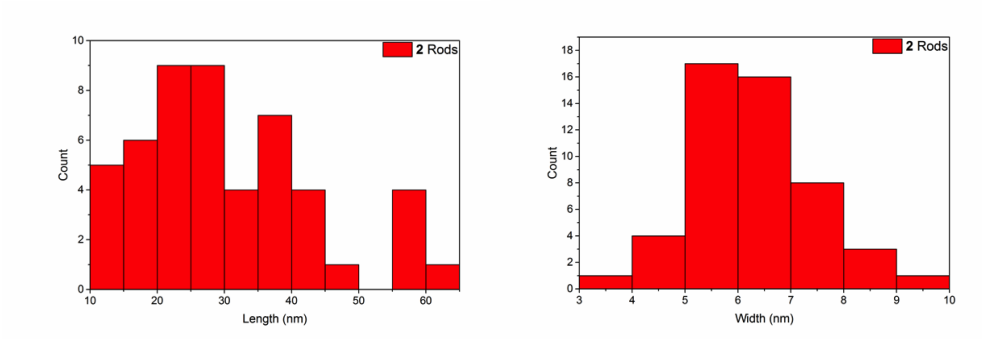

Figure S5.9. Histograms of length (31 ± 13 nm) and width (6 ± 1 nm) distributions measured for **2** (N = 50).

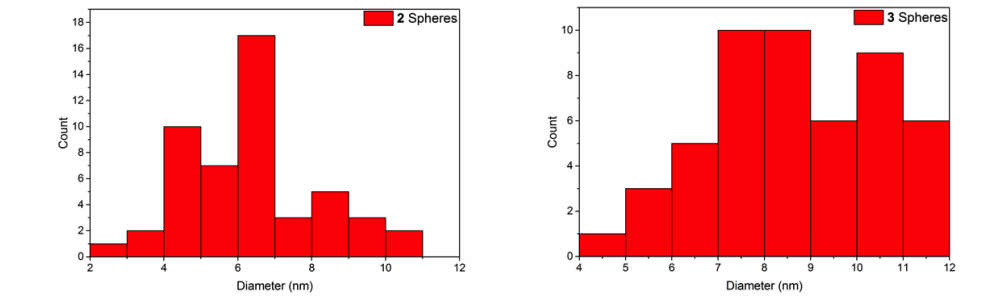

Figure S5.10. Histograms of diameter distributions measured for spherical aggregates of **2** (6 ± 2 nm)(left) and **3** (9 ± 2 nm) (right) (N = 50).

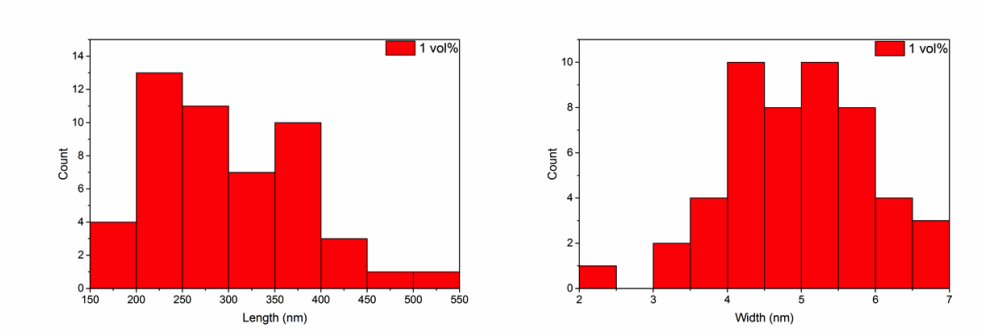

Figure S5.11. Histograms of length (299 ± 78 nm) and width (5 ± 1 nm) distributions measured for **1** at 1 v/v% of carp serum (N = 50).

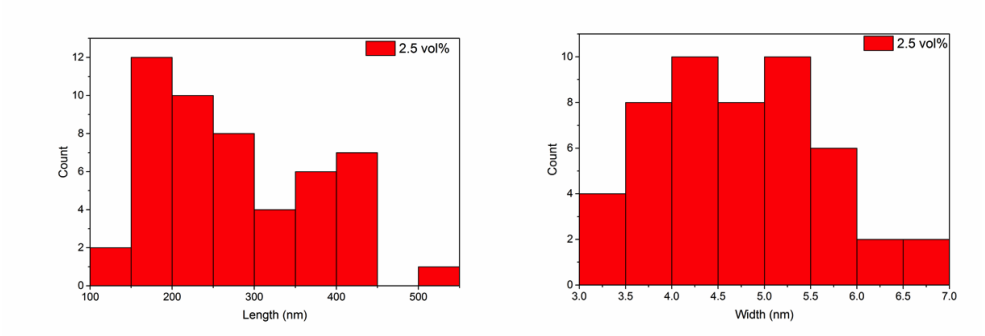

Figure S5.12. Histograms of length (277 ± 103 nm) and width (5 ± 1 nm) distributions measured for **1** at 2.5 v/v% of carp serum (N = 50).

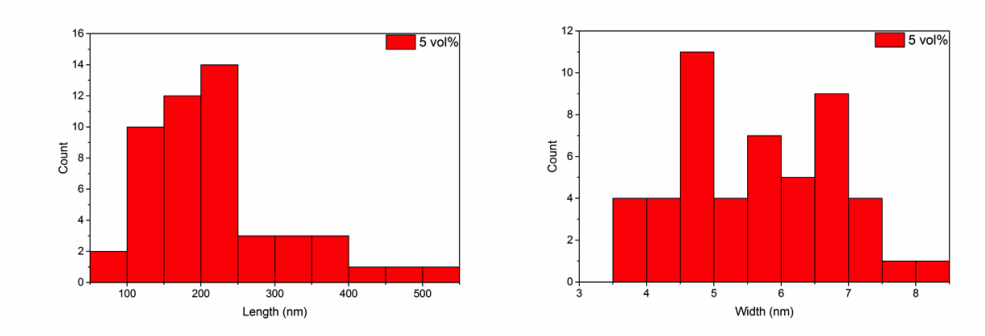

Figure S5.13. Histograms of length (218 ± 96 nm) and width (6 ± 1 nm) distributions measured for **1** at 5 v/v% of carp serum (N = 50).

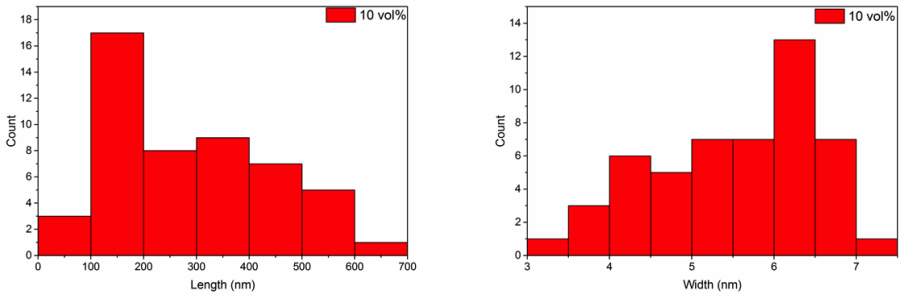

Figure S5.14. Histograms of length (288 ± 142 nm) and width (6 ± 1 nm) distributions measured for **1** at 10 v/v% of carp serum (N = 50).

5.6.9 Whole embryo zebrafish imaging

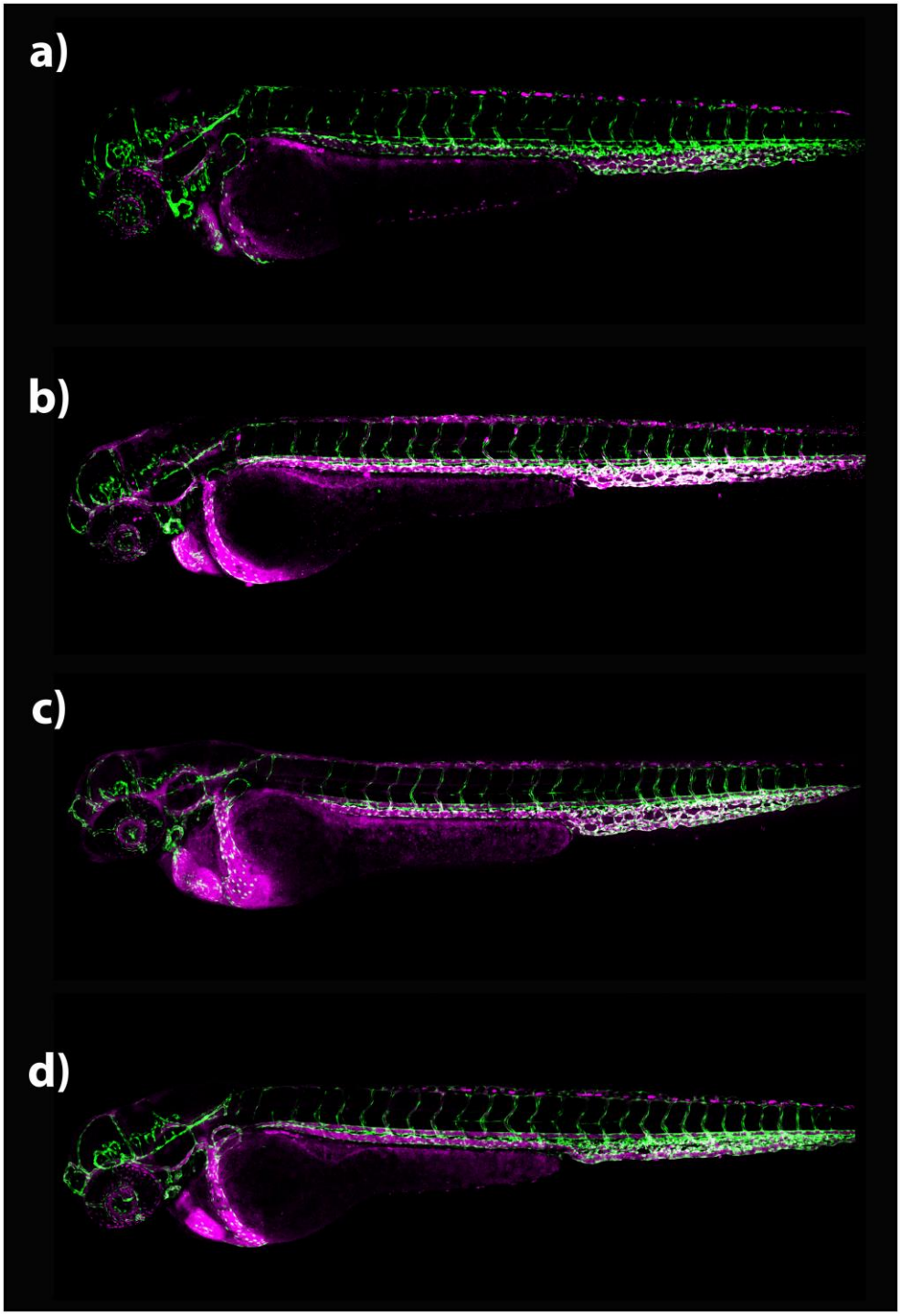

Figure S5.15. Biodistribution of the fluorescently-labeled squaramide-based supramolecular polymer nanoparticles in the zebrafish. Whole-embryo view **1** hour post-injection in the Duct of Cuvier with **1** (a), **2** (b) and **3** (c) (c= 2 mM) co-assembled with 2 mol% **4** in an embryonic zebrafish (*kdrl:GFP*) at 54 hpf. (d) Whole-embryo view after 1 hour injection in the Duct of Cuvier with **4** (c = 40 μM) on its own in an embryonic zebrafish (*kdrl:GFP*) at 54 hpf. This control experiment is carried out to track the biodistribution of the negatively charged monomer itself.

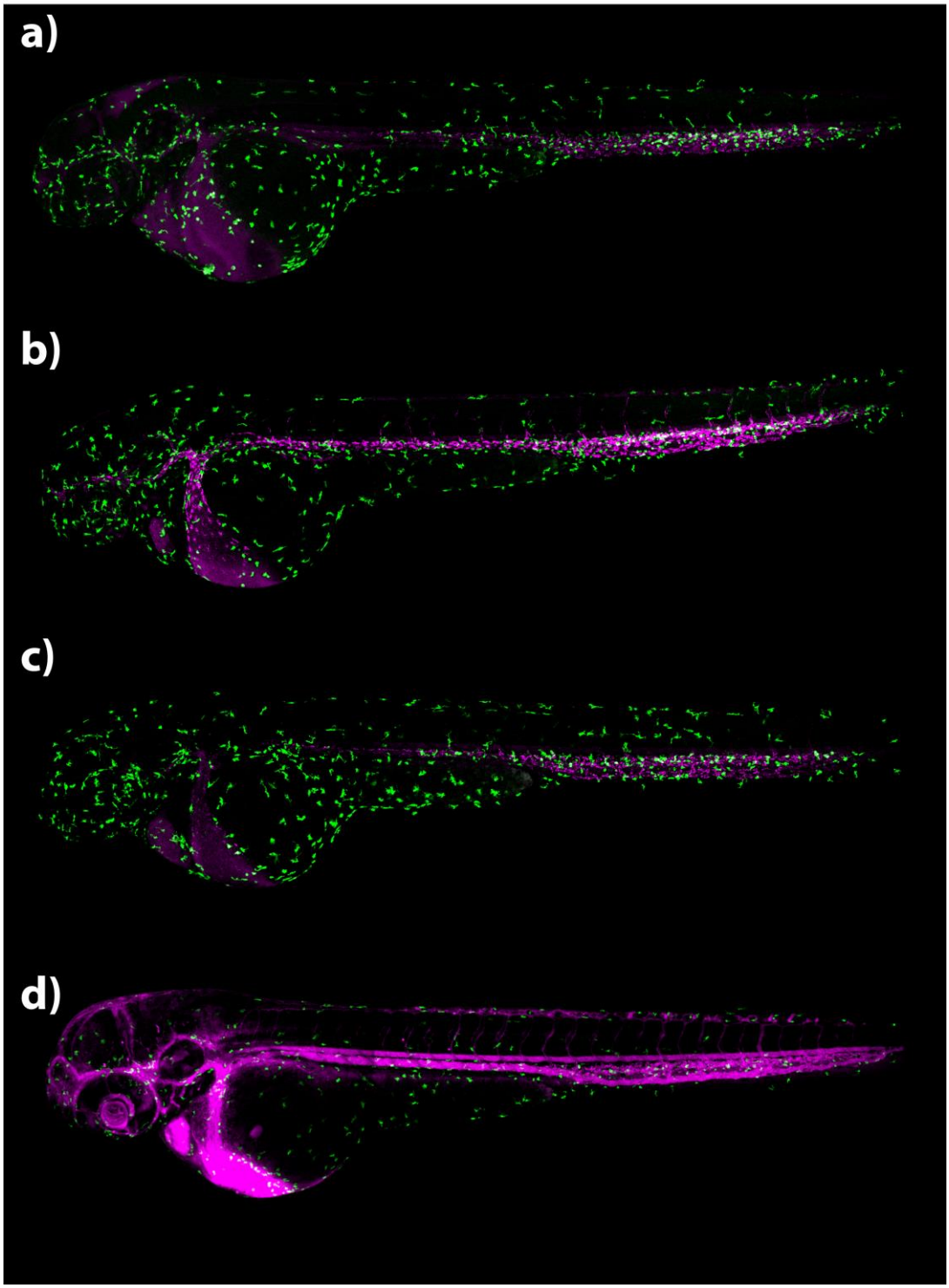
a)
b)
c)
d)

Figure S5.16. Uptake studies of the fluorescently-labeled squaramide-based supramolecular polymer nanoparticles by macrophages in the zebrafish. Whole-embryo view 1 hour post-injection in the Duct of Cuvier with **1** (a), **2** (b) and **3** (c) (c = 2 mM) and 2 mol% of **4** in an embryonic zebrafish (mpeg1:GFP) at 54 hpf. (d) Whole-embryo view after 1 hour injection in the Duct of Cuvier with **4** (c = 40 μM) on its own in an embryonic zebrafish at 54 hpf. This control experiment is carried out to track the uptake of the negatively charged particles of **4** by macrophages studies in zebrafish.

5.6.10 References

(1) Saez Talens, V.; Englebienne, P.; Trinh, T. T.; Noteborn, W. E. M.; Voets, I. K.; Kieltyka, R. E. *Angew. Chemie - Int. Ed.* **2015**, *54* (36), 10502–10506.

(2) Dardonville, C.; Fernandez-Fernandez, C.; Gibbons, S. L.; Ryan, G. J.; Jagerovic, N.; Gabilondo, A. M.; Meana, J. J.; Callado, L. F. *Bioorganic Med. Chem.* **2006**, *14* (19), 6570–6580.